




Review

Towards Construction of the “Periodic Table” of 1-Methylbenzotriazole

Christina Stamou ¹, Zoi G. Lada ², Sophia Paschalidou ³, Christos T. Chasapis ^{4,*} and Spyros P. Perlepes ^{1,2,*}
¹ Department of Chemistry, University of Patras, 26504 Patras, Greece; xrstamou@gmail.com

² Institute of Chemical Engineering Sciences, Foundation for Research and Technology-Hellas (FORTH/ICE-HT), Platani, P.O. Box 1414, 26504 Patras, Greece; zoilada@iceht.forth.gr

³ Laboratory of Inorganic Chemical Technology, Department of Physical Sciences and Applications, Hellenic Army Academy, Vari, 19442 Athens, Greece; spashalidou@sse.gr

⁴ Institute of Chemical Biology, National Hellenic Research Foundation, 11635 Athens, Greece

* Correspondence: cchasapis@eie.gr (C.T.C.); perlepes@upatras.gr (S.P.P.)

Abstract: Metal complexes of benzotriazole-type ligands continue to attract the intense interest of many inorganic chemistry groups around the world for a variety of reasons, including their aesthetically beautiful structures, physical properties and applications. 1-methylbenzotriazole (Mebta) is the *N*-substituted archetype of the parent 1*H*-benzotriazole. The first attempt to build a “periodic table” of Mebta, which includes its complexes with several metal ions, is described in this work. This, at first glance, trivial ligand has led to interesting results in terms of the chemistry, structures and properties of its metal complexes. This work reviews the to-date published coordination chemistry of Mebta with Mn(II), Fe(II), Fe(III), Co(II), Ni(II), Cu(I), Cu(II), Zn(II), Pd(II), Au(I) and {U^{VI}O₂}²⁺, with emphasis on their preparations, reactivity, structures and properties. Unpublished results from our group comprising other Co(II), Ni(II), Cu(II) and Zn(II) complexes, as well as Cd(II), Hg(II), Ag(I), In(III) and Sn(IV) ones are briefly reported. Mebta can also provide access to 1D and 3D heterometallic thiocyanato-bridged Co(II)/Hg(II) and Ni(II)/Hg(II) compounds. In almost all cases, Mebta behaves as a monodentate ligand with the nitrogen of position 3 of the azole ring as the donor atom. However, there are two copper complexes in which this molecule adopts a bidentate bridging coordination behavior. Our efforts to complete the “periodic table” of Mebta are continued.

Keywords: benzotriazole-type ligands; coordination chemistry; 1-methylbenzotriazole metal complexes; reactivity; synthesis; structures



Citation: Stamou, C.; Lada, Z.G.; Paschalidou, S.; Chasapis, C.T.; Perlepes, S.P. Towards Construction of the “Periodic Table” of 1-Methylbenzotriazole. *Inorganics* **2024**, *12*, 208. <https://doi.org/10.3390/inorganics12080208>

Academic Editors: Moris S. Eisen and Gabriel García Sánchez

Received: 20 June 2024

Revised: 14 July 2024

Accepted: 23 July 2024

Published: 30 July 2024



Copyright: © 2024 by the authors. Licensee MDPI, Basel, Switzerland. This article is an open access article distributed under the terms and conditions of the Creative Commons Attribution (CC BY) license (<https://creativecommons.org/licenses/by/4.0/>).

1. Introduction

In the last 15 years or so, there has been a renaissance in the coordination chemistry of benzotriazoles (Figure 1, left) [1], a rather old family of ligands [2], for a variety of reasons (*vide infra*). The aim of this comprehensive review is to provide a synthetic and structural “flavor” of the coordination chemistry of 1-methylbenzotriazole (Mebta; Figure 1, right), the *N*-substituted archetype of 1*H*-benzotriazole (btaH). Over the past three decades, we have been trying to build a “periodic table” of Mebta (for a recent article in this journal, see ref. [3]), by preparing complexes with as many metal and metalloid ions as possible. The spaces (positions) in this “periodic table” contain ions, whose complexes with Mebta *have been structurally characterized by single-crystal X-ray crystallography*; thus, their composition and molecular and crystal structures are known without any doubt. Sporadically, Mebta complexes that have been characterized *only* by spectroscopic methods will be mentioned. Most of the complexes reported so far come from our group, hence the relatively large number of self-citations.

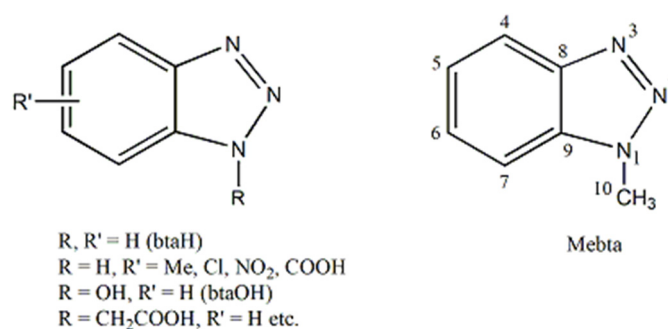


Figure 1. (Left) The structural formula 1H-benzotriazole (btaH) and its derivatives. (Right) The structural formula of 1-methylbenzotriazole (Mebta), the subject of this review.

The emphasis of this review is on the preparation and molecular structures of the metal complexes; in a few cases, a brief note on their spectroscopic characteristics and physical properties will appear. Our intention is to avoid long (and most often boring) preparative descriptions and, for this reason, we shall present the syntheses using balanced chemical equations written in their molecular (and not ionic) format; this representation is correct only if there is one metal-containing product in the reaction (which is probably not always the case). The molecular structures shown are of two types. Some will be illustrated in a schematic way. Other structures have been created from the corresponding CIFs which have been deposited with the Cambridge Crystallographic Data Center (CCDC). For the description of the coordination modes of the ligands involved, the now well-established “Harris Notation” [4] will be used. In a few cases, and for clarity reasons, the ligation modes will be also represented in a schematic way with the coordination bonds drawn with bold lines. Since the description of structures and spectroscopic features/physical properties will be brief, we assume that the readers of this article have a satisfactory background in structural chemistry, spectroscopy and elementary molecular magnetism.

This review is divided into sections. Since Mebta is a ligand, Section 2 provides the reader with some historical information and the utility of ligands in modern inorganic chemistry. Section 3 describes the important role of benzotriazoles in various branches of chemistry with emphasis on their coordination chemistry. Section 4 gives some information concerning the organic, physical and theoretical chemistry of free Mebta. Sections 2–4 are the “hors d’oeuvre” of the review article. Sections 5 and 6 will be the “main menu” of our scientific meal. Section 5 describes the so-far published coordination chemistry of Mebta; we have chosen to arrange our discussion according to the metal justifying the term “periodic table”. Section 6 is a brief overview of the unpublished results on the topic by our group. Finally, some preliminary conclusions and perspectives on the metal chemistry of Mebta will be presented.

An excellent review of recent advances in the coordination chemistry of benzotriazole-based ligands is available [1]; this has limited information about complicated N1- and N2-substituted benzotriazoles with substituents containing other donor groups, but without any citation of Mebta. An informative review on metal complexes of triazoles and tetrazoles also appeared in ref. [5], with a limited description of the coordinating properties of a few benzotriazoles but again with no mention of Mebta. Thus, this article appears to be the first review describing the coordination chemistry of Mebta.

2. Ligands in Coordination Chemistry

Metal ions and ligands are the necessary ingredients of coordination chemistry. Perhaps most inorganic chemists do not know that the word “ligand” and its concept were unknown to Alfred Werner [6]. The term “ligand” (Latin *ligare*, to bind) was introduced in 1917 by Alfred Stock to describe the groups bonded to boron, carbon and especially silicon. The word did not come into use among English-speaking chemists until the Second World War. Between the two world wars the term was used by Klement in a German journal [7],

and by 1940 Tsuchida and Tumaki were using it often in descriptions of coordination complexes [8,9]. The popularity of Jannik Bjerrum's PhD Thesis made the term "ligand" widely accepted by scientists publishing in English and American journals. It was officially introduced by IUPAC in the inorganic chemistry nomenclature in the late 1950s [10].

Coordination chemistry is a living branch of chemistry, continuously evolving and generating new concepts and challenges in bonding and structure. Ligands are at the core of inorganic, supramolecular and nanoscale chemistry, and the proper utilization of known ligands and the design of new ones is behind many exciting developments. Theoretical concepts related to them [11] are the chelate effect, the macrocyclic effect, the cryptate effect, the conformation of chelating rings, chirality, the isoelectronic and isolobal relationships and the reactivity of coordinated ligands, among others.

3. Benzotriazoles in Several Branches of Chemistry

1*H*-benzotriazole or more strictly 1*H*-benzo[1,2,3]triazole (btaH; R = R' = H in Figure 1, left) and its derivatives belong to the class of heterocycles known as azoles; these ligands, especially 1*H*-imidazole, have been central "players" in the development of modern coordination and bioinorganic chemistry after 1970. Benzotriazoles contain two fused 6-(benzene) and 5-(1,2,3-triazole) rings. The parent molecule (btaH) exists in two tautomeric forms, the benzenoid form (Figure 2, left) and the quinonoid form (Figure 2, right); the former is more stable than the latter (by ca. 10 kcal mol^{−1}) accounting for its presence more than 99.9% at equilibrium. This difference has been attributed to the much higher dipole moment (ca. 4.5 D) of 1*H*-benzotriazole (benzenoid) than that of its 2*H* (quinonoid) tautomer (ca. 0.4 D). The result of this difference is that most derivatives appear as the N(1)-isomer [12]. If the steric bulk of the *N*-substituent increases, the proportion of the N(2)-isomer becomes higher [12]. The btaH molecule has weak acidic (p*K*_a = 8.2) and extremely weak basic (p*K*_b < 0) properties; due to these characteristics, it is soluble both in bases (e.g., aqueous Na₂CO₃) and acids (e.g., hydrochloric acid of various molarities), but it is insoluble in H₂O.



Figure 2. The two tautomeric forms of btaH.

The popularity of btaH among *organic chemists* is tremendous [13–16], mainly thanks to the pioneering research of Alan Katritzky; when he passed away in 2014, he had published ca. 640 papers on the chemistry, properties and technological aspects of benzotriazoles. Today, this number exceeds 700! Among the properties that make btaH extremely useful in organic chemistry are its non-toxicity (in small quantities), low cost, very good solubility in a variety of organic solvents, easy synthesis and chemical (e.g., in the presence of H₂SO₄, NaOH, LiAlH₄, etc.) and thermal (its ring system is stable up to 400 °C) stability. Another important feature of synthetic utility is that btaH is both electron donating and electron attracting; the former characteristic results in acyl, aroyl, phosphonyl and sulfonyl derivatives, while the latter can stabilize carbanions. The benzotriazolate anion (bta[−]) is a good leaving group and it can be used in place of halogen substituents in many reactions, because the benzotriazolyl derivatives are more stable than their halogen analogues [15]. Concerning the derivatives of btaH, 1-hydroxybenzotriazole (btaOH; R = OH and R' = H in Figure 1) is an extremely useful auxiliary in the synthesis of peptides [15].

In the related field of *medicinal chemistry*, benzotriazoles play an important role. They exhibit antimicrobial, antiparasitic, choleric, cholesterol-lowering and even antitumor properties [17,18]. Transition-metal complexes of benzotriazoles are also candidates for the development of antitumor agents. Copper(II) complexes can be functional models of the copper-zinc-superoxide dismutase (Cu, Zn-SOD). According to the theory of Buettner and

Oberley [19], SOD activity in tumor cells is lower than that in healthy cells. Complexes **1** and **2** (Figure 3) showed very low and very high SOD activities, respectively. Since these compounds differ only in the position of the substitution of the benzotriazole ring, it is obvious that the biological activity depends on the structural characteristics of the coordinated ligand. Complex **2** exhibits an in vitro SOD activity with a $0.06 \mu\text{M}$ IC_{50} value, comparable with results reported for other SOD-mimicking agents. In accordance with these data, the evaluation of the in vitro cytotoxicity on several tumor lines showed that **2** is much better than **1** with IC_{50} values in the $13\text{--}28 \mu\text{M}$ range.

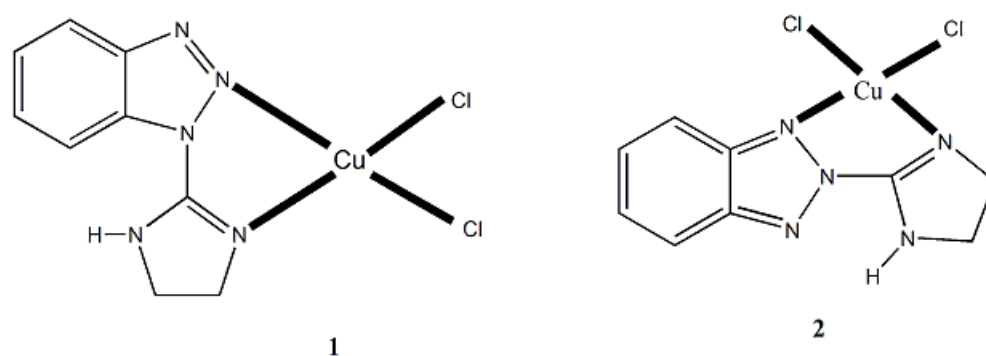


Figure 3. Two Cu(II) complexes with closely related benzotriazole ligands with low (**1**) and high (**2**) in vitro antitumor activities; see text for discussion.

Benzotriazole and its derivatives also attract the intense interest of *environmental scientists*. Polar benzotriazoles, e.g., btaH, btaOH and compounds substituted (Me-, Cl-, -NH_2 etc.) at position 5 of the benzene ring are characterized as emerging pollutants in aqueous media [20], where they exist in low concentrations; their presence in such systems arises from their uses (*vide infra*). Because of their high aqueous mobility, which is a consequence of their polarity, they have been detected in rivers, lakes, groundwater, snow, wastewater (treated and untreated) and, unfortunately, in drinking water. Their presence has also been confirmed in soil air, house dust, textiles, plants and human urine. Several techniques have been used for their separation from a variety of matrices, such as classical liquid–liquid extractions, microextraction methods and solid-phase extraction, the latter being the most important.

Benzotriazole chemistry is also related to many aspects of *material science*. Thus: (a) Benzotriazole-decorated graphene oxide is a valuable material for successful removal of U(VI) from nuclear waste water [21]. Using 5-methylbenzotriazole-modified graphene oxide, a high removal capacity of 264 mg/g for U(VI) was achieved at pH 3.5. (b) Several btaH derivatives have been successfully tested for energetic material applications [22–24]. These contain amino, azide and/or nitro substituents at the benzene ring, combined sometimes with nitro-containing 6-membered aromatic ring substituents on the azole system (Figure 4). Such nitrogen-rich compounds contain a large number of N–N and C–N bonds, and their energetic potential derives from the N_2 formation during combustion. For example [24], the compounds 5-amino-4-nitro-1*H*-benzo[1,2,3]triazole (left in Figure 4) and 5-azido-4-nitro-1*H*-benzo[1,2,3]triazole (middle in Figure 4) have densities of 1.61 and 1.62 g cm^{-3} , detonation velocity values of 5.70 and 5.45 km s^{-1} and detonation pressures of 13.4 and 12.4 GPa , respectively, all comparable to the classical energetic material 2-methyl-1,3,5-trinitrobenzene (TNT). (c) *Ortho*hydroxyphenyl benzotriazoles are among the best ultraviolet absorbers (stabilizers) and find use as additives in coatings, paints, adhesives, plastic materials, food packing films and personal care products. These compounds absorb the destructive UV radiation from sunlight and dissipate the energy in the form of heat generating a thermally excited ground-state species [25–27]. The mechanism of excited-state deactivation has been proposed to be due to an excited-state intramolecular proton transfer (ESIPT). The molecules contain a strong intramolecular H bond which is essential for their photostability; (d) 1*H*-benzotriazole and its polar derivatives are excellent corrosion

inhibitors for metals (mainly Cu) and their alloys [28–32]. Procter and Gamble patented btaH as an inhibitor in 1947 [33]. For this reason, they find widespread applications in aircraft de-icing fluids, antifreeze liquids, detergents for household uses in dishwashing machines and in a variety of industrial systems (cooling, breaking, cutting, etc.). Most importantly, btaH and some of its derivatives, e.g., a mixture of 4-methylbenzotriazole and 5-methylbenzotriazole (with the market name tolyltriazole), are used in the treatment (for protection against further corrosion) of metal-based artifacts of archaeological and historical importance, the first report dating back in 1967 [34]. Today this mixture is effective for the storage of corroded objects and in the preservation of stabilized antiquities [35,36]. The exact mechanism of btaH action on copper materials has not yet been elucidated [29,31]. It is generally accepted [28] that the inhibition is achieved through the complexation of the deprotonated inhibitor molecules and the species in the metal surface (e.g., oxides), thus resulting in strong Cu-N bonds and in the formation of a compact surface film.

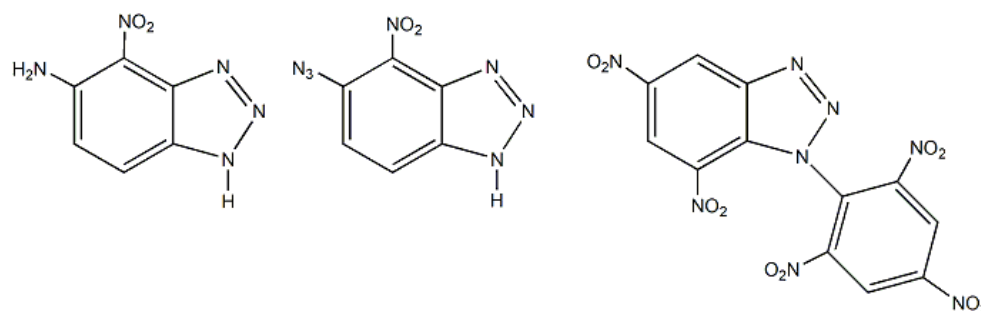


Figure 4. The benzotriazole derivatives 5-amino-4-nitro-1H-benzo[1,2,3]triazole (**left**), 5-azido-4-nitro-1H-benzo[1,2,3]triazole (**middle**) and 5,7-dinitro-1-(2',4',6'-trinitrophenyl)benzo[1,2,3]triazole (**right**) which are efficient energetic materials.

The *physical chemistry* (including theoretical studies) and spectroscopy of benzotriazoles have also attracted the intense interest of researchers [12,37–45]. Thus, their ¹H, ¹³C and ¹⁵N NMR spectra have been studied in depth [38,39,42]. Early theoretical studies provided an explanation for the great difference in stability between btaH and 1,2,3-triazole [12]. The electronic structures and relevant stabilities of *N*-substituted benzotriazoles were studied by UV photoelectron spectroscopy, in combination with high-level ab initio methods [40], and the *N*-substituent effects were shown to depend on the mode of attachment of the substituent to the benzotriazole skeleton. Surface-enhanced Raman spectroscopic studies of benzotriazoles on copper electrodes have been also performed to investigate the nature of the adsorbates at the metal/solution interface and address issues of corrosion inhibition by these compounds [43–45].

Benzotriazole and benzotriazole-based compounds have been used as primary ligands in *coordination chemistry*, albeit less than the triazole ligands. In general, these ligands are redox “innocent”. The parent compound and its C-substituted derivatives can be deprotonated and bridge up to three metal ions [1]. The to-date crystallographically established coordination modes of such bta[−] ligands are illustrated in Figure 5. Benzotriazolate-type compounds are suitable ligands for the synthesis of coordination clusters, which often contain other chelating ancillary ligands, with aesthetically beautiful structures [46–56] and metal topologies, e.g., cyclic cages and kuratowski-type molecules. The deprotonated ligands can also act as linkers towards the construction of coordination polymers [57–74]. A perusal of references [46–74] reveals that benzotriazole (and its C-substituted with no donor groups derivatives) confirms that these ligands form, in the solid state, complexes with a variety of s-, p-, d- and f-block metal ions. When additional donor groups are present on the azole (e.g., R = OH and R' = H in Figure 1, left) or benzene (e.g., R = H and R' = COOH) rings, the bridging capabilities of the resulting ligands increase, often leading to clusters [55,56] or polymers [60–67,69–74] which sometimes exhibit interesting physical (optical, magnetic, ...) properties. Examples in cluster chemistry include compounds [MZn₄Cl₄(L)₆] (M^{II} = Zn, Fe, Co, Ni, Cu; L[−] = the 5,6-dimethylbenzotriazolate anion) represented by the nonplanar K_{3,3}

graph [50], $[\text{Fe}^{\text{II}}_3\text{Zn}_6\text{Cl}_6(\text{L}')_{12}]$ (L' = the 5,6-dimethoxybenzotriazolate anion) which exhibits the thermal spin-crossover behavior [49] and $(\text{DMFH})[\text{NaHg}^{\text{II}}_4(\text{bta})_6\text{I}_4]$ which is photoluminescent [51]. Examples in the coordination polymer area include $\{[\text{Cu}(\text{btaO})_2(\text{MeOH})]\}_n$ (btaO^- is the deprotonated 1-hydroxybenzotriazole; $\text{R} = \text{OH}$ and $\text{R}' = \text{H}$ in Figure 1, left), which was the first molecular Cu^{II} soft magnet reported [74], and the 2D coordination polymer $\{[\text{Zn}(\text{L}'')(\text{py})_2]\}_n$ (L'' = the doubly deprotonated benzotriazole-5-carboxylic acid, $\text{R} = \text{H}$ and $\text{R}' = \text{COOH}$ in Figure 1, left; py = pyridine) which is a highly selective and sensitive luminescent sensor for PO_4^{3-} and Cu^{2+} ions in aqueous media [70].

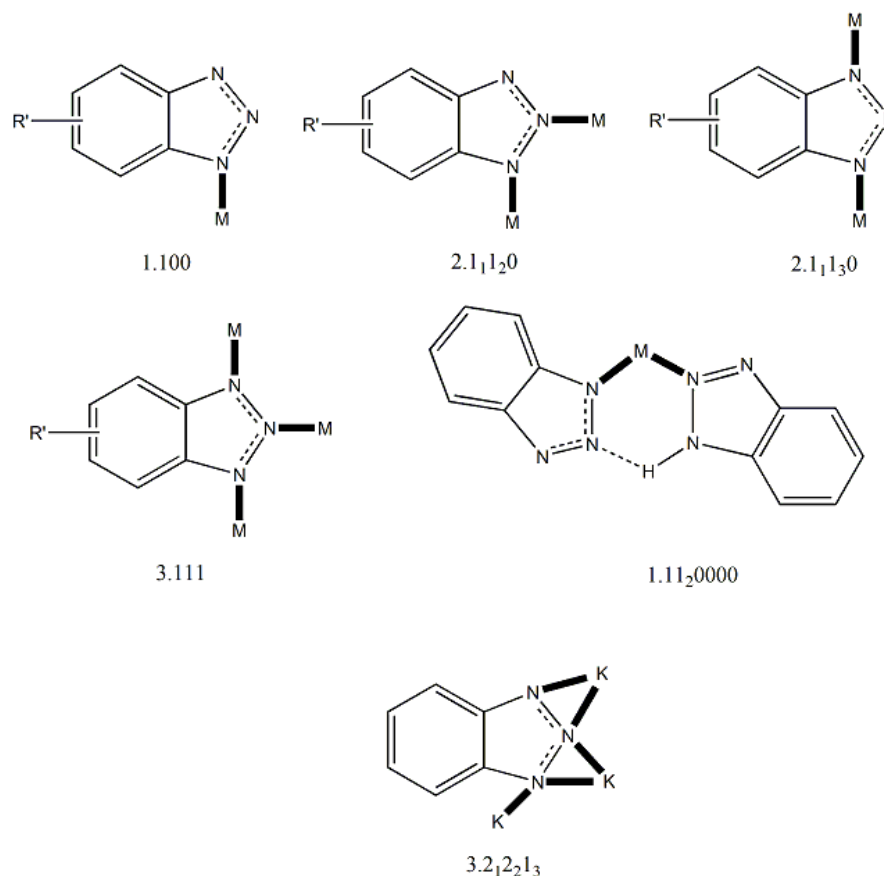


Figure 5. The to-date crystallographically observed coordination modes of the deprotonated C-substituted benzotriazoles and the Harris notation that describes these modes; R' is a non-donor group. The coordination bonds are drawn with bold lines. The dashed lines indicate delocalization and the dotted line represents a H bond. The $(\text{btaHbta})^-$ anion, illustrated in the bottom right of the figure, can be formally described as a neutral (btaH) and an anionic (bta^-) benzotriazole and acts as a N, N'-bidentate “chelating” ligand (pseudo chelating), considering that the $\text{N}\cdots\text{H}$ interaction is part of a 6-membered ring.

4. 1-Methylbenzotriazole: The “Free” Organic Compound

1-methylbenzotriazole (Mebta; Figure 1, right) is the archetype of N-substituted benzotriazoles with non-donor substituents. Mebta is a cream solid (almost white). It is moderately harmful to the respiratory system, dangerous if ingested and causes irritation upon contact with the skin and the eyes.

Mebta is synthesized by the methylation of btaH with MeI in MeOH under strongly alkaline conditions [75,76], but it is also available in the market. The compound is readily soluble in most organic solvents and insoluble in H_2O . It is readily dissolved in HCl , HBr , HI , HNO_3 and HClO_4 acids, from which the corresponding salts can be isolated. Its NMR δ values are as follows. ^1H NMR: 8.06 (d, H4); 7.86 (d, H7); 7.57 (t, H6); 7.42 (t, H5); 4.34 (s, H10). $^{13}\text{C}[^1\text{H}]$ NMR: 127.6 (C6); 133.5 (C9); 145.3 (C8); 110.7 (C7); 124.0 (C5); 119.1 (C4); 34.2

(CH₃). These values (in ppm) are from our own data in *d*₆-DMSO and are in agreement with those reported in the literature [3,38,39,42,75,76]. The ¹⁵N NMR signals in the same solvent appear at δ-161.5 (N1), -1.1 (N2) and -41.0 (N3) ppm [39]. Recently, Marinakis' group studied the IR, Raman, UV/Vis, ¹H and ¹³C NMR spectra of Mebta using experimental and computational methods [77]. DFT calculations using various functionals and basis sets were employed to model the experimental data. The experimental vibrational and NMR data were in excellent agreement with the theoretical predictions. The solvation of the compound in various solvents (MeOH, MeCN, DMF, DMSO) was also studied through UV/Vis spectroscopy experiments and time-dependent DFT calculations.

The crystal structure of Mebta was unknown. Very recently, Edelmann's group investigated the reactivity of the stable *N*-heterocyclic nitrenium salt 1,3-dimethyl-1,2,3-benzotriazolium iodide, (Me)₂bta⁺ I[−] (which is prepared by treatment of Mebta with an excess of MeI) towards nucleophilic reagents [78]. Strong nucleophiles, e.g., KH, potassium cyclopentadienide (Kcp), NaOMe, KO^tBu and NaSEt, all reacted with (Me)₂btaI leading to demethylation and back-formation of crystals of Mebta; the yields of the reactions were in the range 80–90% (Figure 6). The reactions with NaOMe and NaSEt require high temperatures (reflux), whereas those with the other nucleophiles proceed at 20 °C. As expected, the nine atoms of the condensed two-ring system are perfectly in a plane, confirming the aromaticity of Mebta. In agreement with this, the −CH₃ group bonded to N1 is twisted out of the plane by only 7 °C. The N1–N2–N3 angle is 109.4°. Due to resonance stabilization, the N–N bond lengths are in the range between the typical values of single and double bonds. The N1–N2 bond (1.36 Å) is longer than the N2–N3 (1.31 Å), implying a higher double-bond character for the latter.

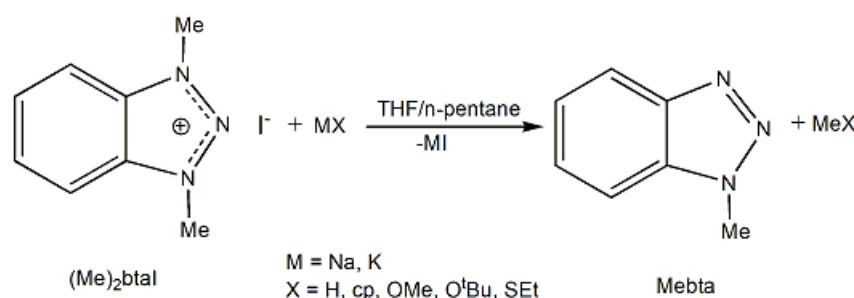


Figure 6. Demethylation reactions of the stable nitrenium salt (Me)₂btaI with strong nucleophiles to give crystalline Mebta.

5. The Published Coordination Chemistry of 1-methylbenzotriazole

5.1. Is Mebta a Boring Ligand?

At first glance, the answer to this question is “yes”. In the great majority of Mebta metal complexes (with one published exception, *vide infra*) the molecule behaves as a monodentate ligand, the donor atom being the N atom of position 3 of the azole ring (Figures 1 and 7, left).

The almost exclusive N(3)-coordination of Mebta has been explained using *ab initio*-level (MP2) calculations in EtOH solution of the compound (EtOH is an often used solvent for the preparation of its metal complexes) [3]. The calculated negative neutral atomic charges are $q_r = 0.31 \text{ |e|}$ for N3 and $q_r = -0.04 \text{ |e|}$ for N2, strongly implying that N3 should be the preferable center for the attack of Mebta by metal ions. This terminal monodentate ligation has been related to the inability of Mebta to act as a corrosion inhibitor for copper and its alloys [45,79]. Thus, Mebta can be considered a typical aromatic monodentate N-donor, like pyridine. From another viewpoint, the answer to the titled question is “no”. The reasons are the unique steric and electronic properties of Mebta, and the recent discovery [80] (see also Section 6) that Mebta is capable of bridging two metal ions in a 2.1₂1₃0₁ (or simply 2.110) manner (Figure 7, right). Most complexes with N(3)-coordination of Mebta have different chemistry (composition, structures, properties) compared with those of the typical ligands with one N donor atom, even if the ancillary inorganic ligands

(Cl^- , Br^- , NO_3^- , N_3^- , ...) or counterions (ClO_4^- , PF_6^- , BF_4^- , CF_3SO_3^- , ...) are the same! The Mebta complexes appear also different from those of the closely related 1-methyl-1,2,3-triazole (Meta, Figure 8), although the number of reported metal complexes of the latter is extremely small (*vide infra*).

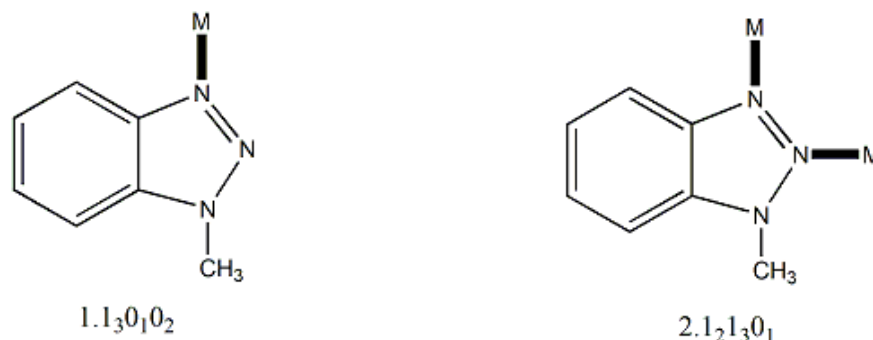


Figure 7. The to-date crystallographically confirmed coordination modes of Mebta in its metal complexes and the Harris notation that describes these modes. The $1.1_30_10_2$ mode (**left**) has been observed in almost all of its complexes, and the $2.1_21_30_1$ (**right**) in only two cases. The coordination bonds are drawn with bold lines.

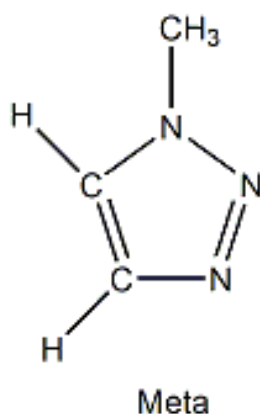
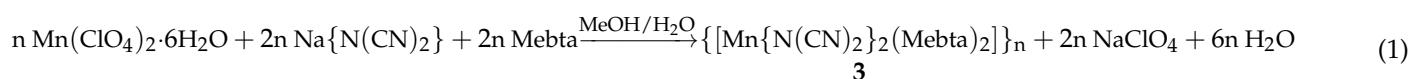


Figure 8. The structural formula of 1-methyl-1,2,3-triazole and its abbreviation.

5.2. An 1D Mn(II)/Mebta Coordination Polymer from the Use of the Dicyanamido Ligand

The dicyanamide ion, $\text{N}(\text{CN})_2^-$, is a popular inorganic ligand that often behaves as a bridging group leading to 1D, 2D and 3D coordination polymers with aesthetically beautiful molecular structures and interesting topological features. An aqueous $\text{Mn}^{\text{II}}/\text{N}(\text{CN})_2^-$ solution, prepared in situ from the reaction between $\text{Mn}(\text{ClO}_4)_2 \cdot 6\text{H}_2\text{O}$ and $\text{Na}\{\text{N}(\text{CN})_2\}$, was layered with a methanolic solution of two equivs. of Mebta; slow mixing of the solutions resulted in the isolation of needle-like colorless crystals of $\{[\text{Mn}\{\text{N}(\text{CN})_2\}_2(\text{Mebta})_2]\}_n$ (**3**) in low to moderate yield ($\leq 30\%$), Equation (1).



Complex **3** consists of linear 1D chains in which two neighboring Mn^{II} centers are bridged by two $\mu(1,5)\text{-N}(\text{CN})_2^-$ ($2.1_11_50_3$) groups via the terminal nitrile nitrogen atoms; two N(3)-coordinated ancillary Mebta ligands complete the distorted octahedral coordination sphere at each metal ion which lies on an inversion center resulting in N-Mn-N angles of 180° (Figure 9). The $\text{Mn}^{\text{II}} \cdots \text{Mn}^{\text{II}}$ distance is $\sim 7.46 \text{ \AA}$. Variable-temperature (2–300 K) dc magnetic susceptibility studies revealed a very weak antiferromagnetic exchange interaction between the $S = 5/2$ metal ions, typical for $\mu_2(1,5)\text{-N}(\text{CN})_2^-$ ligands.

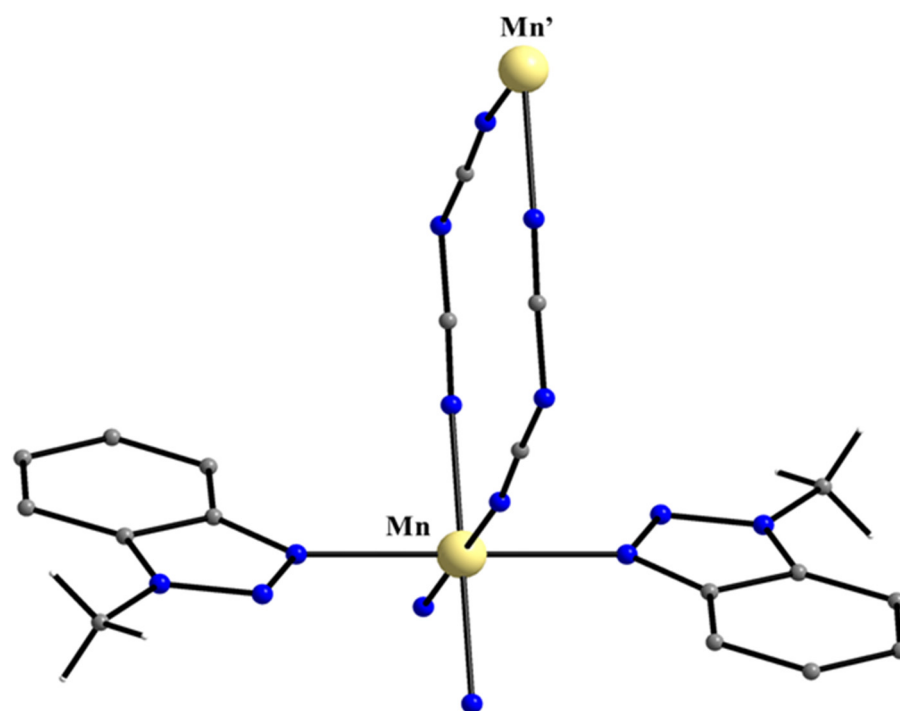
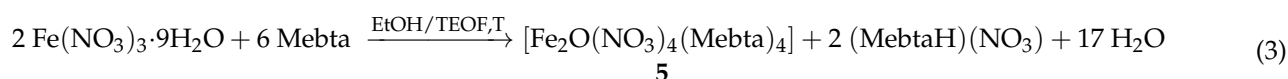
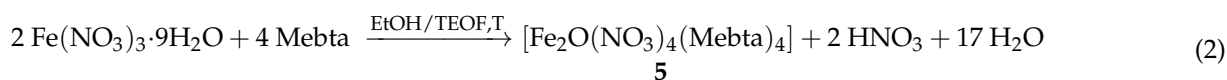


Figure 9. A view of **3** emphasizing the coordination sphere of one Mn^{II} atom.

5.3. Fe(II) and Fe(III) Complexes

Complex $\{[\text{Fe}\{\text{N}(\text{CN})_2\}_2(\text{Mebta})_2]\}_n$ (**4**) was prepared using the same approach as **3** in a slightly higher yield (~45%). The two complexes are isomorphous [81]. The Fe^{II}...Fe^{II} distance is ~7.39 Å and a weak antiferromagnetic interaction was observed.

The 1:2 reaction between Fe(NO₃)₃·9H₂O and Mebta in EtOH/triethyl *ortho*formate (TEOF) under reflux gave an orange solid, recrystallization of which from MeNO₂ produced crystals of [Fe₂O(NO₃)₄(Mebta)₄] (**5**) in a 55% yield [82], Equation (2). The dehydrating agent TEOF (*vide infra*) is necessary to remove most of the water contained in EtOH and in the iron(III) starting material, thus avoiding hydroxo precipitates. The produced HNO₃ would be expected to attack the oxo bridge and decompose the product. This does not happen because the protons produced from water could be neutralized by Mebta which does not react. In accordance with this, the yield never exceeds 55%, meaning that Mebta and an unknown iron(III) species remain in solution. If this assumption is correct, the formation of **5** can be represented by Equation (3).



The crystal structure of **5** consists of isolated centrosymmetric dinuclear molecules [Fe₂O(NO₃)₄(Mebta)₄] (Figure 10). The two Fe^{II} centers are distorted octahedral bonded to the bridging oxo group, two N(3)-coordinated Mebta molecules, and one bidentate chelating (1.110) and one monodentate (1.100) nitrate group. The Fe^{III}...Fe^{III} distance is 3.54 Å. The Fe-O(nitrate) bond *trans* to the oxo group (2.28 Å) is longer than its counterpart in the *cis* position (2.10 Å), a consequence of the powerful *trans* influence of the short Fe-μ₂(O) bond. The two bulky, planar Mebta ligands are *trans* to each other, thus minimizing steric interaction. The Mebta groups in *syn* positions are nearly parallel. There are intradimer stacking interactions between these ligands on the two sides of the molecule [82]. The ν_{as}(Fe-O-Fe) vibration appears at 851 cm⁻¹ in the IR spectrum of the complex. The

$\nu_s(\text{Fe-O-Fe})$ mode occurs at 384 cm^{-1} in the FT-Raman spectrum and it shifts to 375 cm^{-1} upon ^{18}O substitution. Magnetic data indicate strongly antiferromagnetically coupled high-spin diiron(III) species. The ^{57}Fe -Mössbauer spectrum of **5** at 4.2 K in zero field consists of a single quadrupole doublet with $\delta = 0.50\text{ mm s}^{-1}$ (vs. metallic Fe at room temperature) and $\Delta E_Q = 1.30\text{ mm s}^{-1}$, values typical for an oxo-bridged octahedral complex in an O/N environment.

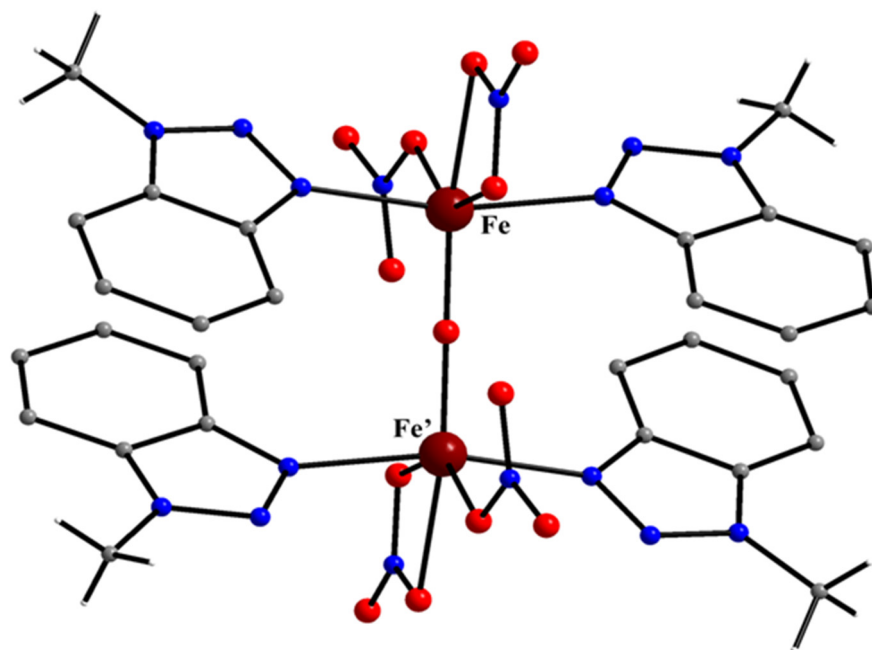
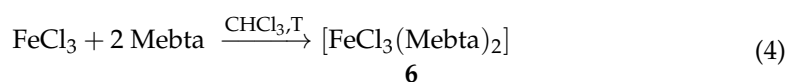


Figure 10. The molecular structure of the dinuclear complex **5**.

Changes in the inorganic starting material from $\text{Fe}(\text{NO}_3)_3 \cdot 9\text{H}_2\text{O}$ to FeCl_3 and the solvent from EtOH to CHCl_3 affect the chemical and structural identity of the product. The 1:2 reaction of FeCl_3 and Mebta in refluxing CHCl_3 gave the yellow product $[\text{FeCl}_3(\text{Mebta})_2]$ (**6**) in typical yields of 55–60%, Equation (4) [83]. Excess of Mebta led again to complex **6**.



The molecule (Figure 11) of **6** possesses a crystallographically imposed two-fold axis of symmetry passing through the Fe^{III} and a Cl atom. The metal ion is surrounded by three terminal chloro ligands and two nitrogen atoms from two planar N(3)-coordinated Mebta molecules. The five donor atoms define a slightly distorted trigonal bipyramid around Fe^{III} with the two Mebta nitrogens at the axial sites. The Fe-N bond distances (2.18 \AA) are somewhat long, and this is due to atom–atom repulsions between the donor nitrogen atoms and the chloro groups ($\sim 3.10\text{ \AA}$). The crystal structure of **6** is stabilized by intermolecular π - π stacking interactions between the Mebta ligands, each $[\text{FeCl}_3(\text{Mebta})_2]$ molecule interacting with four of its neighbors.

The far-IR spectrum of **6** shows one strong terminal metal ion-chloro stretch, $\nu(\text{Fe-Cl})_t$, at 378 cm^{-1} and one weaker Fe^{III} -N stretching mode, $\nu(\text{Fe-N})$, at 196 cm^{-1} . A reasonable approximation of the molecular symmetry around Fe^{III} is D_{3h} , and thus one $\nu(\text{Fe-Cl})_t$ (E') and one $\nu(\text{Fe-N})$ (A_2'') mode would be expected. Molar conductivity data ($25\text{ }^\circ\text{C}$, 10^{-3} M) indicate that the complex is non-electrolyte in MeCN; surprisingly **6** is a 1:1 electrolyte in MeNO_2 , probably suggesting the presence of $[\text{FeCl}_2(\text{Mebta})_4]^+$ and $[\text{FeCl}_4]^-$ species in solution. The δ and ΔE_Q values in the zero-field ^{57}Fe -Mössbauer spectrum of **6** at room temperature are 0.24 mm s^{-1} and 0.27 mm s^{-1} , respectively. The δ value is typical for high-spin 5-coordinate iron(III). The asymmetry in peak intensity is typical for complexes

having a large positive zero-field splitting parameter, D . The complex has been tested as a homogeneous catalyst (MeCN under N_2) in the presence of the “green” H_2O_2 oxidant; it displays moderate to high catalytic activity towards the oxidation of several alkenes, cyclohexane and n-hexane [83]. The mechanism involves hydrogen abstraction and oxygen transfer in a variety of alkene substrates, resulting in good yields of epoxidation and allyl oxidation products. The products from the cyclohexane oxidation are cyclohexanol, cyclohexanone and 4-hexen-1-ol, and those from n-hexane are hexanones and hexanols.

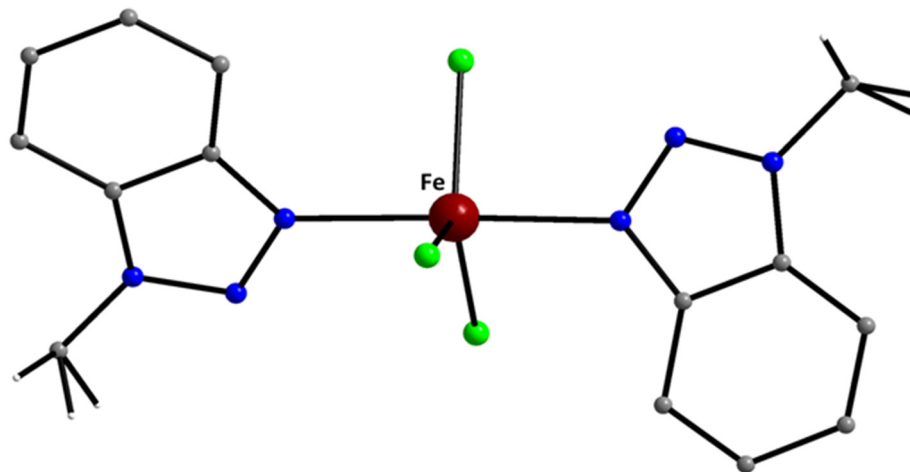
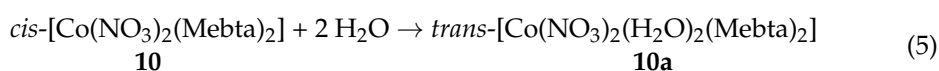


Figure 11. Plot of the molecular structure of **6**.

5.4. Tetrahedral and Octahedral Co(II) Complexes

Complexes $[CoCl_2(Mebta)_2]$ (**7**), $trans-[Co(NCS)_2(Mebta)_4]$ (**8**), $trans-[Co(NCS)_2(MeOH)_2(Mebta)_2]$ (**9**) and $cis-[Co(NO_3)_2(Mebta)_2]$ (**10**) were prepared by simple reactions of Co(II) starting materials ($CoCl_2$, $Co(NCS)_2$, $Co(NO_3)_2 \cdot 6H_2O$) and Mebta in alcohols in moderate to good yields [84]. The metal:ligand molar ratio does not affect the product identity. The reaction of $Co(NCS)_2$ with Mebta in alcohols is solvent-dependent. In MeOH, the product is compound **9**, while the reaction in EtOH or heavier alcohols produces complex **8**. This different behavior may be due to the better coordinating ability of MeOH. Another point of synthetic interest is that the concentration of H_2O in the $Co(NO_3)_2 \cdot 6H_2O$ /Mebta reaction mixture in EtOH has a pronounced effect on the product identity. Only in H_2O -free medium [use of TEOF (*vide infra*) under heating] could compound **10** be isolated. In H_2O -containing ethanolic mixtures, the resulting product was $trans-[Co(NO_3)_2(H_2O)_2(Mebta)_2]$ (**10a**) as evidenced by a poor quality X-ray structure. Since the reaction yields complexes **10** and **10a** if carried out in H_2O -free or H_2O -containing EtOH, respectively, the former can give the latter by the addition of small amounts of water, Equation (5). Contributory factors to the ligand redistribution ($cis \rightarrow trans$) may be the minimization of the total repulsion energy and hydrogen bonding.



There are two crystallographically independent molecules in the structure of **7**; one of them is shown in Figure 12. The structural characteristics of the two molecules are similar. The Co^{II} center is surrounded by two N atoms belonging to two 1.13010₂ Mebta molecules (Figure 7) and two terminal chloro ligands in a slightly distorted tetrahedral geometry. The repulsion between the two chlorides is presumably responsible for the observed distortion. The Cl-Co-Cl plane makes angles of $\sim 85^\circ$ with each of the Mebta planes, while the dihedral angle between the two planar ligands is $\sim 40^\circ$.

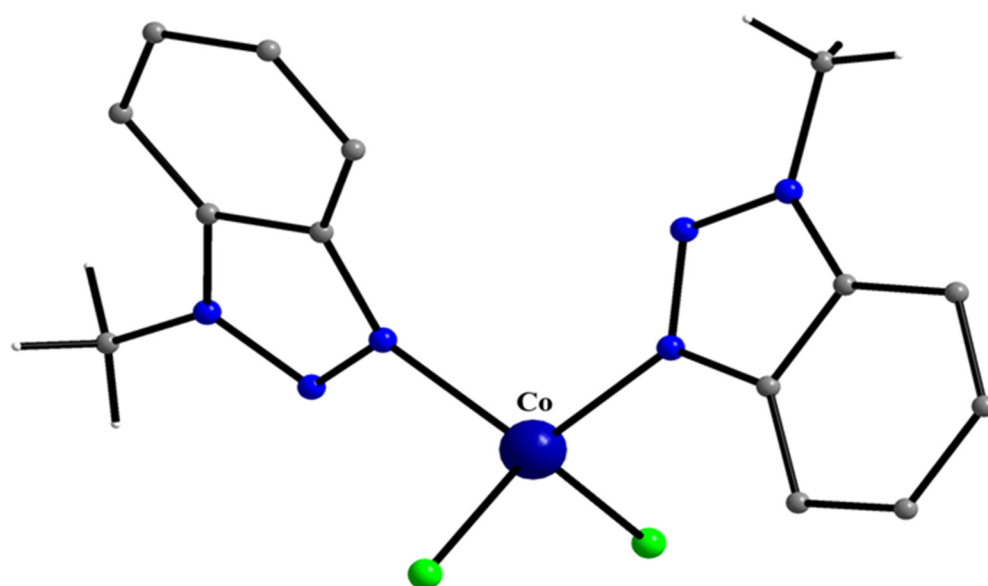


Figure 12. The molecular structure of 7.

The octahedral molecules of 8 and 9 possess a crystallographically imposed center of symmetry. In 8 (Figure 13), the metal ion is coordinated to two isothiocyanato groups and four N(3)-bonded Mebta molecules. In complex 9 (Figure 14), the Co^{II} ion is coordinated by pairs of *trans*-related isothiocyanato groups, MeOH molecules and Mebta ligands. The Co-N and Co-O bond lengths in the two complexes are typical for high-spin electronic configurations. The NCS^- ions are coordinated in a slightly bent fashion ($\text{Co}^{\text{II}}\text{-N}\equiv\text{C} = \sim 165^\circ$). Both methanolic oxygen atoms are involved in intermolecular H bonds with the acceptors being the sulphur atoms of isothiocyanato ligands of neighboring complex molecules.

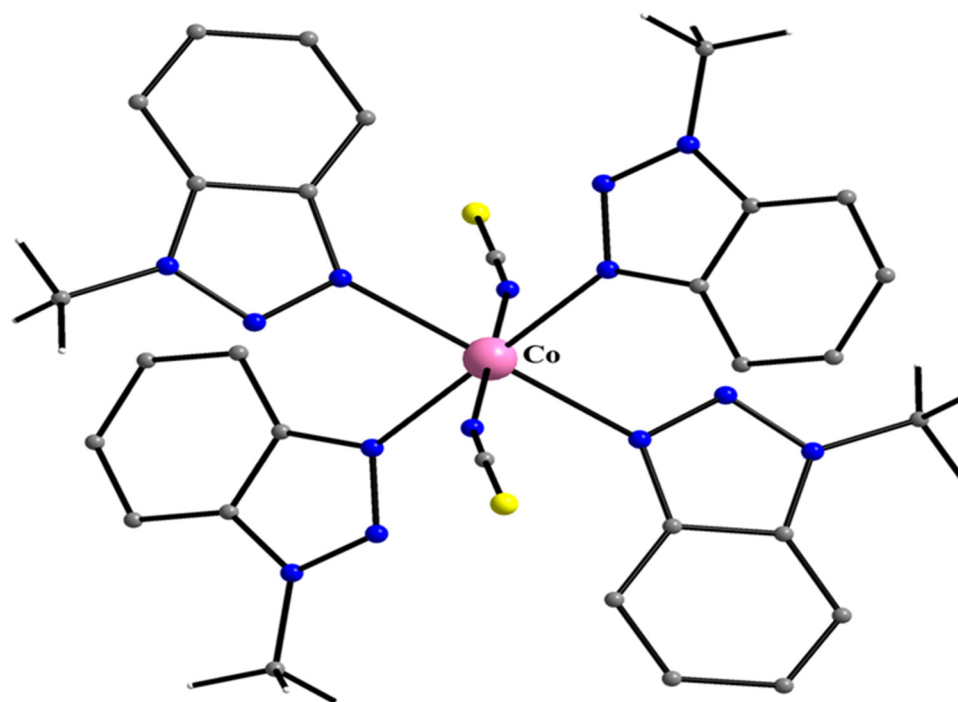


Figure 13. The molecular structure of 8.

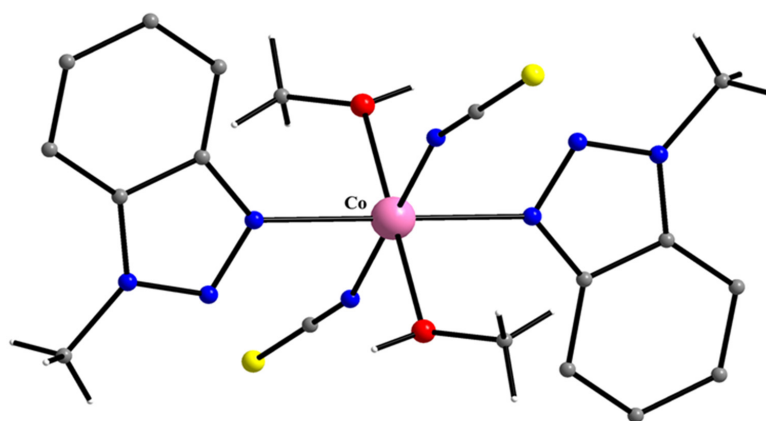


Figure 14. The molecular structure of **9**.

The structure of **10** (Figure 15) consists of well-separated, severely distorted *cis*-[Co(NO₃)₂(Mebta)₂] octahedral molecules with two anisobidentate chelating nitrate groups and two monodentate Mebta ligands. The high spin Co^{II} center lies on a crystallographic two-fold axis (C₂), which bisects the N-Co-N angle. The Co-O bonds *trans* to N atoms (2.28 Å) are longer than those *trans* to O atoms (2.06 Å). This difference in bond lengths is attributed to the fact that in *cis*-bis(bidentate ligand)bis(monodentate ligand) metal complexes, one end of the bidentate ligands is associated with a smaller repulsion energy than the other end. The Co-N bond distance in **10** is noticeably shorter than the corresponding lengths in **8** and **9** (2.05 vs. ~2.18 Å); these distances in **10** are similar to those observed in the tetrahedral complex **7**. This structural feature is reflected in the room-temperature effective magnetic moment, μ_{eff} , value of **10** (4.58 B.M.), which is in the region expected for tetrahedral Co(II) complexes. The explanation is the distorted 6-coordinate structure of C₂ symmetry for **10**; the degeneracy of the Co^{II} ion is lifted [⁴T_{1g}(O_h) → ⁴A, 2 ⁴B in C₂]. The new ground state, being an orbital singlet, gives rise to a magnetic moment closer to the spin-only value than that observed in an octahedral complex (~5 B.M.). The absence of a center of symmetry in **10** also gives a high-intensity d-d spectrum (contrary to normal octahedral complexes) since both p and d orbitals span common representations in C₂. The EPR spectra of **8–10** at various temperatures show typical rhombic g values. The low-temperature data and their temperature dependence are both indicative of a rather large and positive (>15 K) axial zero-field splitting. In the octahedral complex **10a**, the Co^{II} ion is coordinated with pairs of *trans*-related monodentate nitrate, aqua and Mebta ligands.

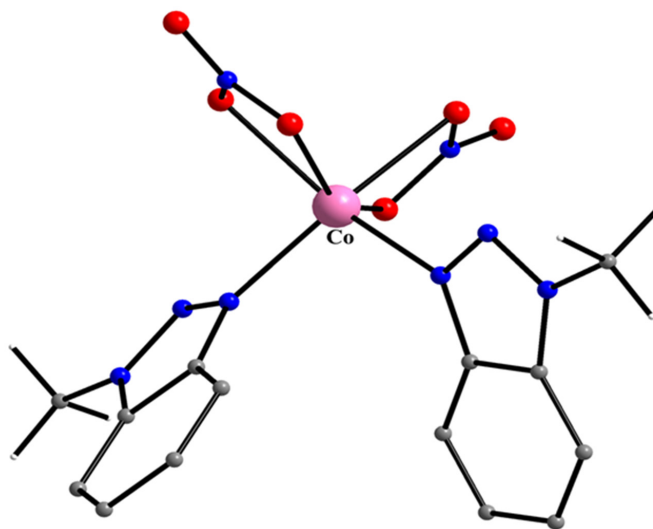


Figure 15. The molecular structure of **10**.

5.5. Reactions of Ni(II) Thiocyanate and Nitrate with 1-methylbenzotriazole

The 1:2 reaction between $\text{Ni}(\text{SCN})_2$ and Mebta in refluxing MeOH gave complex *trans*- $[\text{Ni}(\text{NCS})_2(\text{MeOH})_2(\text{Mebta})_2]$ (**11**) in yields higher than 70% [85]. The complex is isostructural (but not isomorphous) with its Co(II) analogue **9** (Figure 14).

The $\text{Ni}(\text{NO}_3)_2 \cdot 6\text{H}_2\text{O}$ /Mebta reaction system proved to be synthetically and structurally interesting. In the 1:2 reaction mixture, the concentration of H_2O affects the product identity (Figure 16). Complex *cis*- $[\text{Ni}(\text{NO}_3)_2(\text{Mebta})_2]$ (**12**) could be isolated only in H_2O -free [use of TEOF (*vide infra*)] warm ethanolic or acetonic mixtures; the yield was ~70%. Employing a ca. 1 M H_2O concentration in Me_2CO and a ca. 10:1 $\text{H}_2\text{O}:\text{Ni}^{\text{II}}$ molar ratio, the isolated blue-green solid $[\text{Ni}(\text{NO}_3)(\text{H}_2\text{O})_2(\text{Mebta})_2](\text{NO}_3)$ (**12a**) was obtained in a 68% yield. Higher H_2O concentration (1.9 M) and $\text{H}_2\text{O}:\text{Ni}^{\text{II}}$ molar ratio (20:1) gave the blue material *trans*- $[\text{Ni}(\text{H}_2\text{O})_4(\text{Mebta})_2](\text{NO}_3)_2$ (**12b**) in a 52% yield. Since the 1:2 reaction between nickel(II) nitrate and 1-methylbenzotriazole gives complexes **12** and **12a**, **12b** if carried out in H_2O -free or H_2O -containing Me_2CO , we suspected that **12** would react with increasing amounts of H_2O to give **12a** and **12b**; indeed, this turned out to be the case (Figure 16).

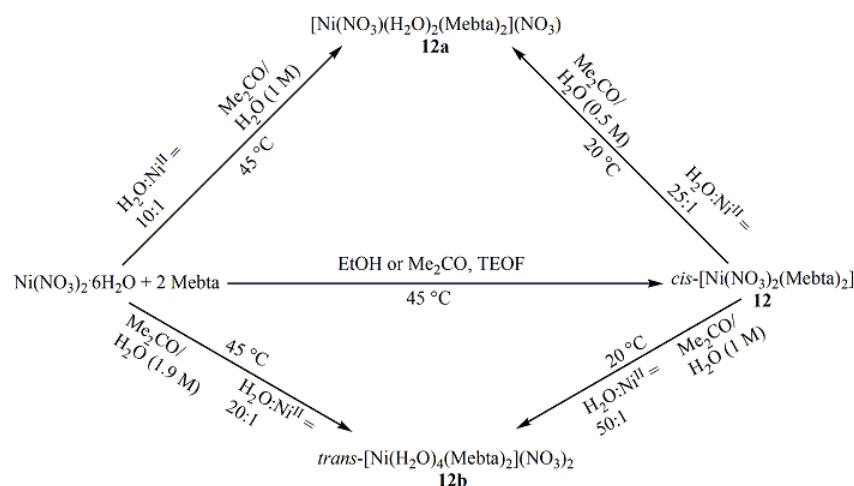


Figure 16. The transformations in the 1:2 $\text{Ni}(\text{NO}_3)_2$ /Mebta reaction mixtures; for more details, see text.

The distorted octahedral complex **12** (Figure 17) is isomorphous with its Co(II) analogue **10** (Figure 15). There are two anisobidentate chelating nitrato groups and two monodentate Mebta ligands, each pair in a *cis* position. The severe distortion of the octahedron is due to the restricted “bite” of the chelating nitrates, with an angle at the metal ion of $\sim 61^\circ$.

A poor single-crystal X-ray data set for **12a** revealed a distorted octahedral cation, with one bidentate chelating nitrato group, two *cis* H_2O molecules and two *cis* Mebta ligands; the 1+ charge of the cation is counter-balanced by a H-bonded ionic NO_3^- . The cation of **12a** can be considered as deriving from the molecule of **12** by replacing a bidentate chelating nitrato group of the latter with two *cis* aqua ligands in the former.

The cation of complex **12b** (Figure 18) has a nearly regular octahedral $\{\text{Ni}^{\text{II}}\text{O}_4\text{N}_2\}$ coordination sphere, involving two centrosymmetrically related Mebta ligands and four H_2O molecules; the two nitrates are ionic. Two of the coordinated H_2O molecules are trigonal and two pseudotetrahedral. In the 3D supramolecular network, each NO_3^- is connected via H bonds with four coordinated H_2O molecules belonging to three different $[\text{Ni}(\text{H}_2\text{O})_4(\text{Mebta})_2]^{2+}$ cations.

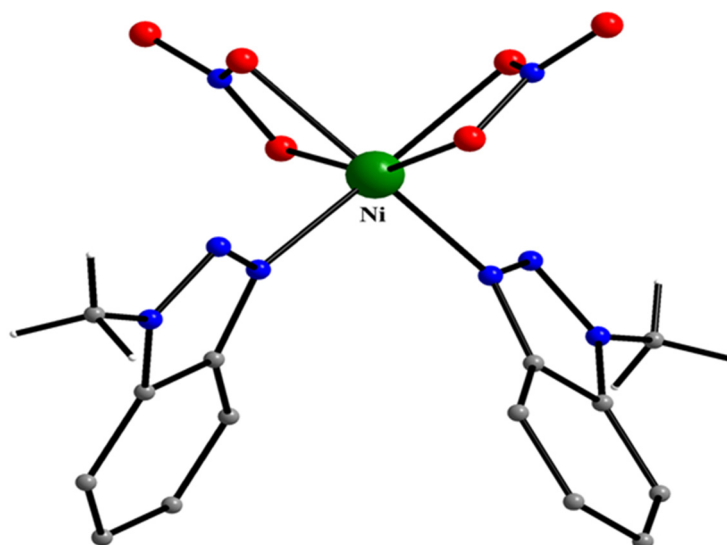


Figure 17. The molecular structure of 12.

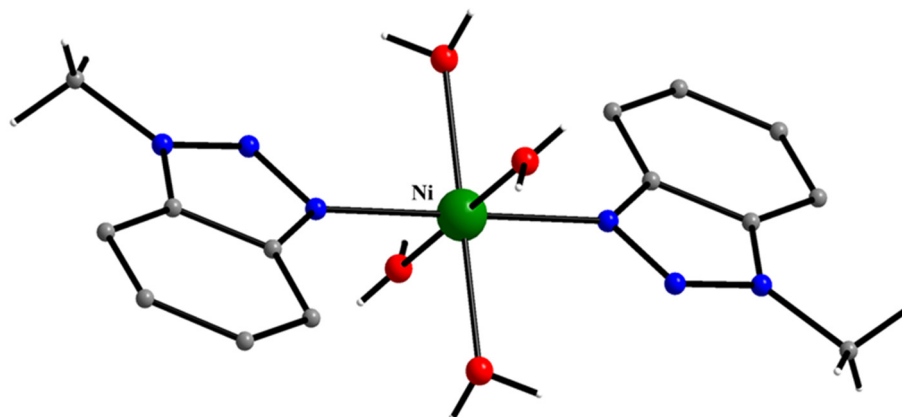
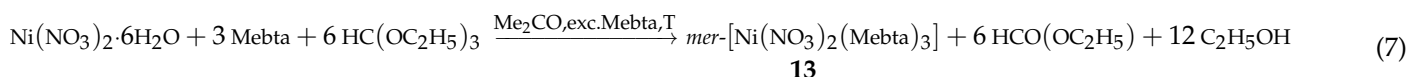
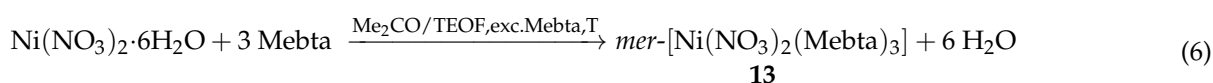


Figure 18. Plot of the $[\text{Ni}(\text{H}_2\text{O})_4(\text{Mebta})_2]^{2+}$ cation that is present in the crystal structure of the salt 12b.

The $\text{Ni}^{\text{II}}:\text{Mebta}$ reaction ratio is also important in the $\text{Ni}(\text{NO}_3)_2 \cdot 6\text{H}_2\text{O}/\text{Mebta}$ system. Employment of a large excess of the ligand ($\text{Ni}^{\text{II}}:\text{Mebta} = 1:12$ and $1:15$) in anhydrous Me_2CO , complex *mer*- $[\text{Ni}(\text{NO}_3)_2(\text{Mebta})_3]$ (**13**), as the mono acetone solvate, could be isolated in moderate yield, Equation (6). A chemically more correct representation of the reaction is shown in Equation (7), which emphasizes dehydration by TEOF; its capacity for H_2O removal increases with increasing temperature. The structure of **13** is shown in Figure 19. The Ni^{II} center is surrounded by three N and three O atoms in a distorted octahedral configuration. The six-coordinate molecule is the *mer* isomer. Both planar nitrates take part in coordination, one as a monodentate ligand and the other as a bidentate ligand. Complex **13** joins only a handful of structurally characterized Ni(II) complexes with both monodentate and bidentate chelating nitrato groups, most of which contain one tridentate chelating organic ligand.



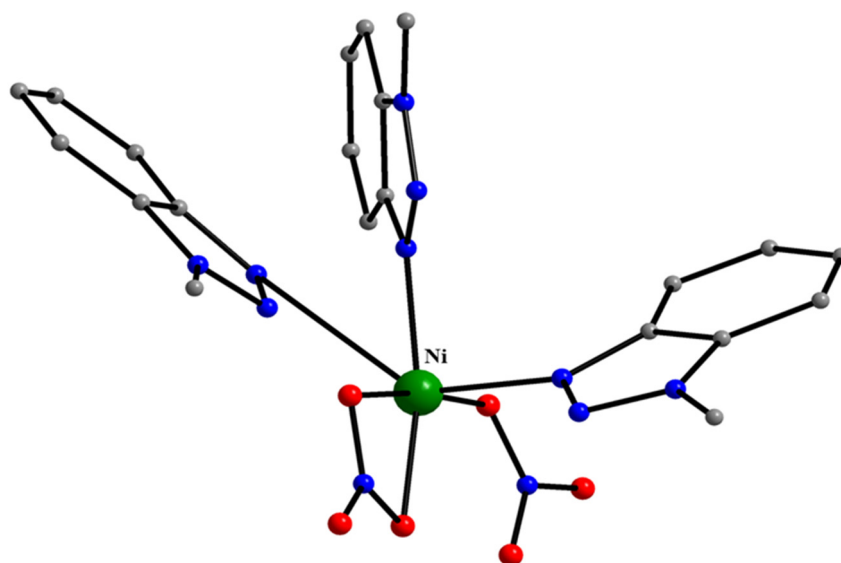
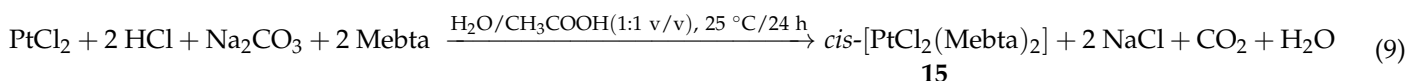
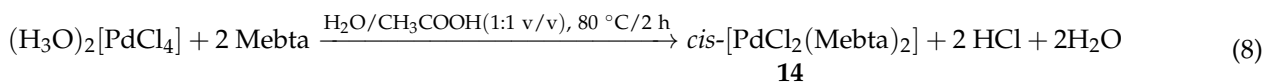


Figure 19. The molecular structure of **13**.

5.6. Square Planar Pd(II) and Pt(II) Complexes

The square planar complexes *cis*-[PdCl₂(Mebta)₂] (**14**) and *cis*-[PtCl₂(Mebta)₂] (**15**) have been prepared by the reactions shown in Equations (8) and (9), respectively; yields of 45–65% were routinely obtained [86].



No X-ray-quality single crystals of the products could be grown. The complexes were characterized by a variety of solid-state and solution physical (conductivity, TG/DTG, pXRD) and spectroscopic (IR, Raman, UV/VIS, ¹H NMR) techniques. Based on these combined studies, *cis* square planar structures were assigned for the two complexes (Figure 20). In particular, the appearance of two $\nu(\text{M-Cl})_t$ (A_1 and B_2 under C_{2v} symmetry) and two $\nu(\text{M-N})$ (A_1 and B_2 under C_{2v}) in both the far-IR and low-frequency Raman spectra of the complexes implies a *cis* configuration (M = Pd, Pt). The *cis* structural type suggests that Cl[−] has a greater *trans* effect compared to Mebta. Apparently, the benzene ring of Mebta near the donor site hampers the arrangement of four Mebta ligands around the metal ion in a square planar environment, and thus preparation of [M(Mebta)₄]Cl₂ ionic complexes is not possible.

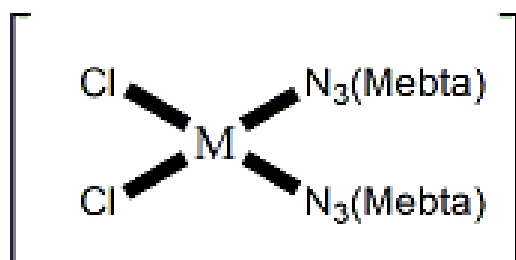


Figure 20. The proposed *cis* square structure of **14** and **15** (M = Pd, Pt). The coordination bonds are represented by bold lines.

5.7. The Rich Coordination Chemistry of Mebta with Cu(II)

Cu(II) is the most studied metal ion in the coordination chemistry of Mebta. Complex $[\text{Cu}(\text{Mebta})_4(\text{H}_2\text{O})](\text{ClO}_4)_2$ (**16**) was readily prepared by the 1:4 reaction of $\text{Cu}(\text{ClO}_4)_2 \cdot 6\text{H}_2\text{O}$ with Mebta in EtOH in ca. 75% yield [87]. The metal coordination geometry in the $[\text{Cu}(\text{Mebta})_4(\text{H}_2\text{O})]^{2+}$ cation (Figure 21) is well described as distorted square pyramidal with the aqua ligand occupying the apical position. Comparison between the structural and spectroscopic properties of **16** and those of the Cu^{II} site of Cu-Zn superoxide dismutase (the enzyme that catalyzes efficiently the dismutation of the harmful superoxide ion to dioxygen and hydrogen peroxide in almost all eukaryotic cells and a few prokaryotes through consecutive reduction and oxidation of the copper ion in the active site) shows that the former can be considered as a fairly good model of the latter. The solid-state and solution electronic spectrum of the complex displays a ligand field band at ~ 675 nm; this d-d absorption maximum is close to that observed for intact $\text{Cu}^{\text{II}}_2\text{Zn}^{\text{II}}_2\text{SOD}$ (680 nm). The X-band EPR spectrum of a polycrystalline sample of **16** at 80 K is typical for axial-type copper(II) compounds with two g values ($g_{\parallel} = 2.245$, $g_{\perp} = 2.060$) and $g_{\parallel} > g_{\perp} > 2.03$, indicating a $d_{x^2-y^2}$ ground state. The enzyme exhibits similar spectral parameters for copper(II) [$g_{\parallel} = 2.271$, $g_{\perp} = 2.083$].

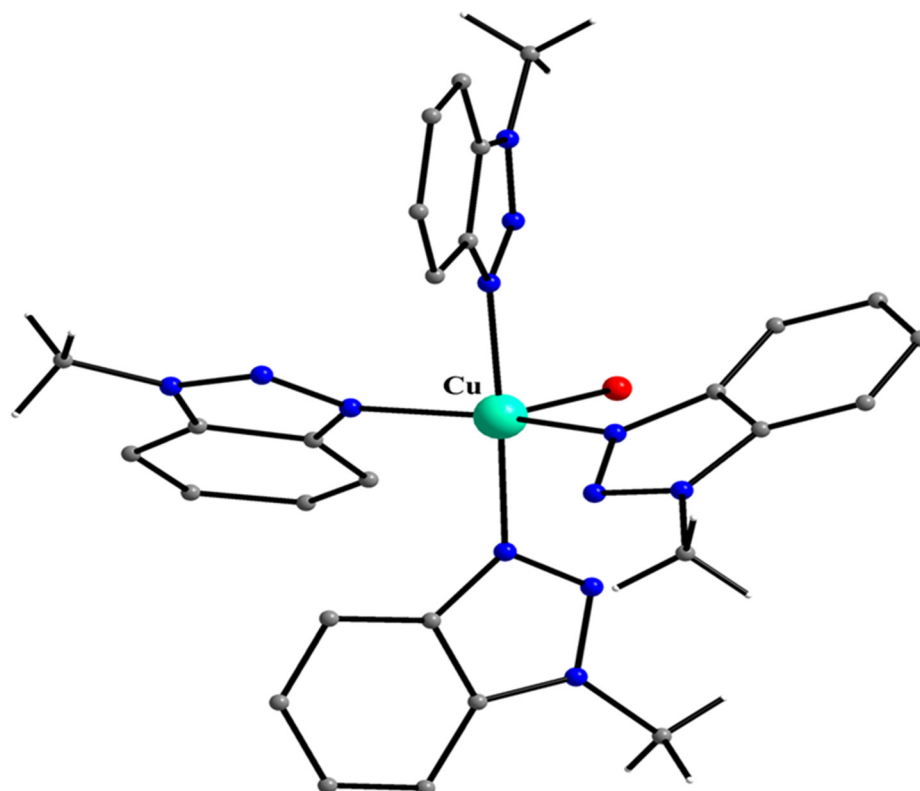
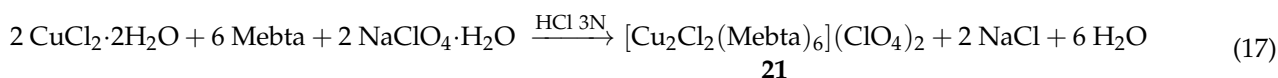
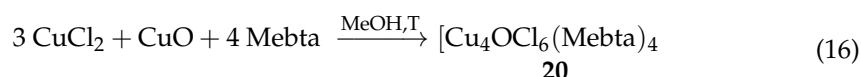
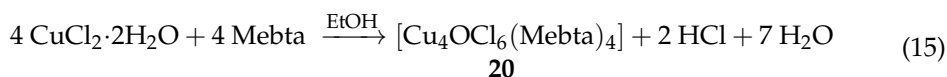
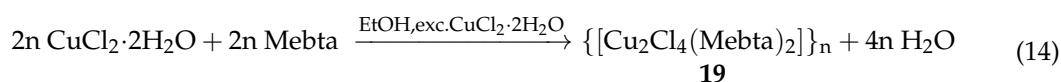
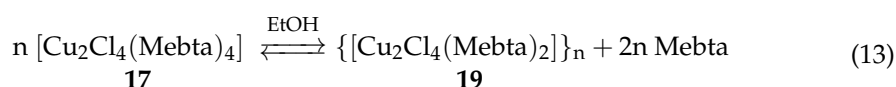
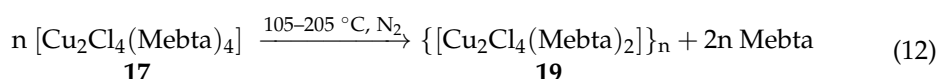
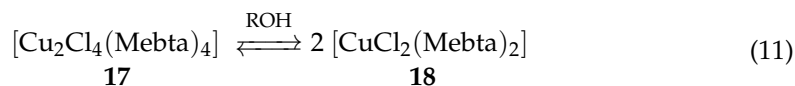
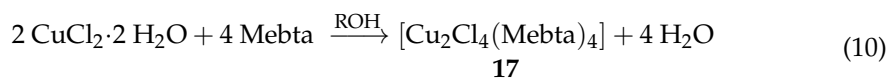


Figure 21. The molecular structure of the cation $[\text{Cu}(\text{Mebta})_4(\text{H}_2\text{O})]^{2+}$ that is present in the crystal structure of **16**.

The $\text{CuCl}_2/\text{Mebta}$ reaction system was proven extremely fertile [88,89]. A systematic investigation of this reaction system, involving the determination of the influence of the $\text{Cu}^{\text{II}}:\text{Mebta}$ ratio, the nature of the solvent and the presence of non-coordinating counterions on the product identity, was carried out by our group [88,89]. As a consequence, complexes $[\text{Cu}_2\text{Cl}_4(\text{Mebta})_4]$ (**17**), $[\text{CuCl}_2(\text{Mebta})_2]$ (**18**), $\{[\text{Cu}_2\text{Cl}_4(\text{Mebta})_2]\}_n$ (**19**), $[\text{Cu}_4\text{OCl}_6(\text{Mebta})_4]$ (**20**) and $[\text{Cu}_2\text{Cl}_2(\text{Mebta})_6](\text{ClO}_4)_2$ (**21**) were isolated and structurally characterized by

single-crystal X-ray crystallography. The various synthetic procedures and transformations are conveniently summarized in the chemical Equations (10)–(17), where R is Me or Et.



Equation (12) represents a solid-state reaction. Concerning Equation (17), our studies indicated that HCl 3N does not take part in the reaction mechanism and merely assists the dissolution of Mebta, in a non-organic solvent system.

The crystal structure of **17** consists of isolated dinuclear molecules $[\text{Cu}_2\text{Cl}_4(\text{Mebta})_4]$ with two bridging chloro groups; a terminal chloride and two *trans* monodentate Mebta ligands complete five-coordination at each metal ion (Figure 22). Due to the presence of a crystallographically imposed inversion center in the middle of the copper(II)⋯copper(II) distance, the bridging $\{\text{Cu}_2\text{Cl}_2\}$ unit is strictly planar. The geometry at each Cu^{II} center is square pyramidal with the apical site being occupied by the chloro group which is basal to the other Cu^{II} in the dimeric molecule. There appear to be intradimer π - π stacking interactions between the nearly parallel *syn* Mebta ligands on the two sides of the molecule. Variable-temperature magnetic susceptibility data indicate a moderate ferromagnetic exchange interaction between the Cu^{II} ($S = \frac{1}{2}$) centers in the dimer and a weak interdimer antiferromagnetic interaction. An insight concerning the effect of structural parameters on the sign and magnitude of the magnetic exchange interactions in **17** and **21** (*vide infra*) was gained through Extended Huckel Molecular Orbital (EHMO) calculations performed on a model system. The calculations have permitted the establishment of a new criterion, holding for magnetostructural correlations in bis(μ -chloro)copper(II) dinuclear complexes [89].

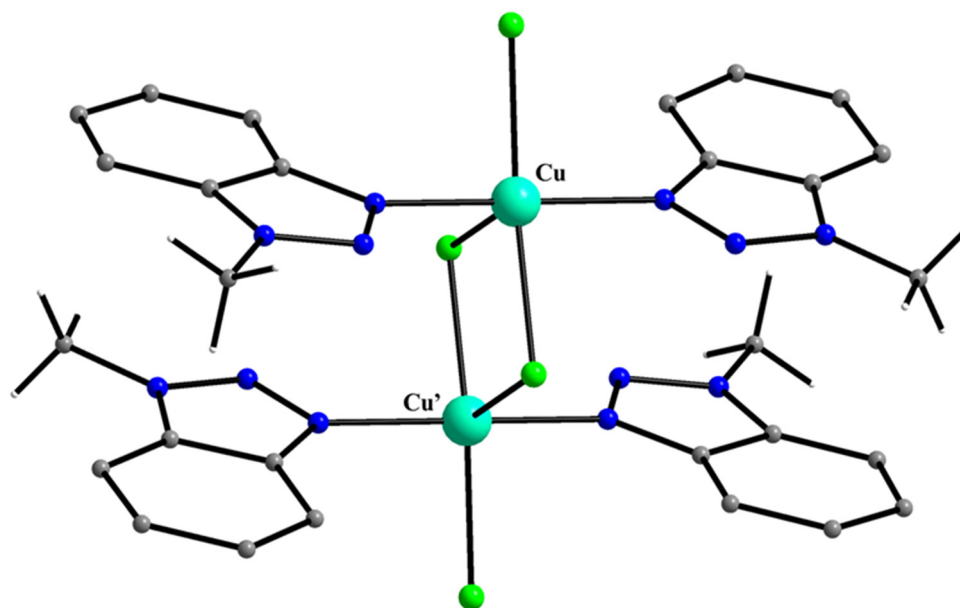


Figure 22. The molecular structure of 17.

The Cu^{II} center in the mononuclear compound 18 (Figure 23) is bonded to two N atoms of the (N3)-coordinated Mebta molecules and two terminal chloro ligands. The coordination geometry can be described as tetrahedrally distorted *trans*-square planar. The *cis* ($93.6\text{--}95.0^\circ$) and *trans* ($143.7\text{--}152.3^\circ$) angles of all donor atoms around Cu^{II} are intermediate between the expected values for tetrahedral (109.5°) and square planar (90° , 180°) coordination, respectively.

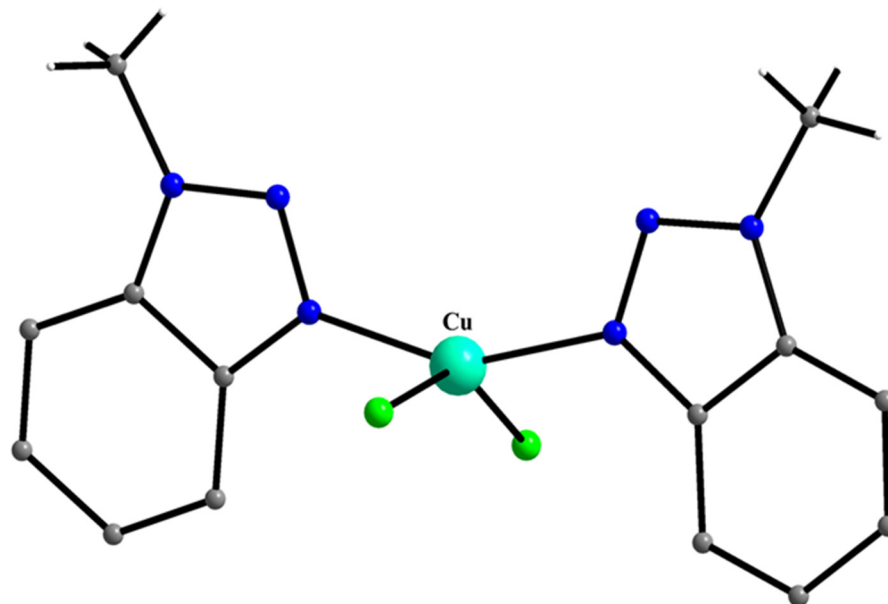


Figure 23. The molecular structure of 18.

The crystal structure of 19 consists of linear, well-separated polymeric chains of Cu^{II} ions bridged asymmetrically by two chloro groups (Figure 24). A regular alternation of two crystallographically non-equivalent metal ions (Cu1 , Cu2) occurs along the chain. Cu1 is bonded to four chloro groups in an almost perfect square-planar arrangement, whereas Cu2 has the *trans*-octahedral $[\text{Cu}(\mu\text{-Cl})_4\text{N}_2]$ environment, the N atoms belonging to two *trans* N(3)-coordinated Mebta molecules. The symmetry elements of the molecular structure (two mirror planes, one two-fold crystallographic axis) are such that each metal

ion is located on a crystallographic center of symmetry. The doubly bridged chain with two alternating coordination spheres observed in **19** is extremely rare in complexes of the empirical formula CuX_2L ($\text{X} = \text{Cl}, \text{Br}$; $\text{L} = \text{monodentate ligand}$). Magnetically, complex **19** behaves as consisting of ferromagnetic chains, which interact antiferromagnetically with the neighboring chains.

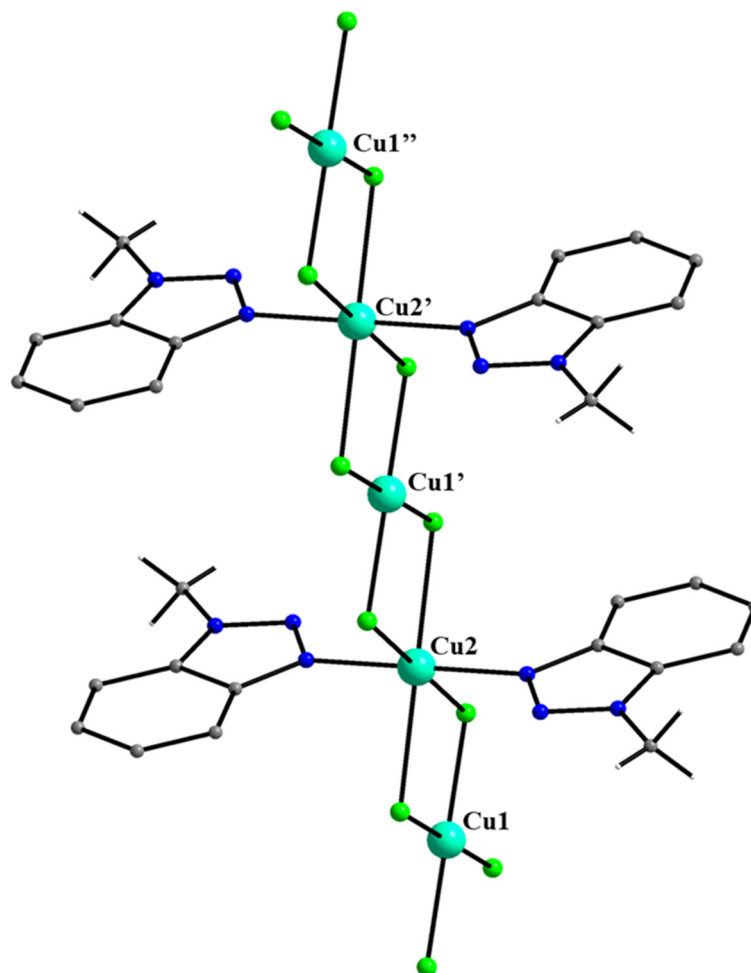


Figure 24. A small portion of one chain that is present in the crystal structure of **19**.

The crystal structure of **20** is composed of tetranuclear $[\text{Cu}_4\text{OCl}_6(\text{Mebta})_4]$ molecules (Figure 25). The molecule contains a tetrahedron of Cu^{II} ions which are held together by one $\mu_4\text{-oxo}$ (O^{2-}) group and six $\mu\text{-chloro}$ ligands; each bridging Cl^- spans an edge of the tetrahedron. One monodentate N(3)-coordinated Mebta molecule is bound to a Cu^{II} ion. Thus, the core is $\{\text{Cu}^{\text{II}}_4(\mu_4\text{-O})(\mu\text{-Cl})_6\}$. The $\mu_4\text{-O}^{2-}$ group and two of the bridging chloro ligands lie on a crystallographic 2-fold axis. The $\text{Cu}_4(\mu_4\text{-O})$ tetrahedron is regular, the Cu-O-Cu angles being 108.6 and 110.9° , and the $\text{Cu}\cdots\text{Cu}$ non-bonding distances varying from 3.10 to 3.15 Å. Angles at the bridging chloro groups are $\sim 81^\circ$. Each of the Cu^{II} centers is in a slightly trigonal bipyramidal coordination environment, with the $\mu_4\text{-O}^{2-}$ group and the Mebta N atom in the two axial positions. The six $\mu\text{-Cl}^-$ groups comprise a distorted octahedron around $\mu_4\text{-O}^{2-}$ ion. The $\text{O}\cdots\text{Cl}$ distances are in the range $2.88\text{--}2.95$ Å and the $\text{Cl}\cdots\text{Cl}$ ones vary between 3.98 and 4.25 Å; the *cis* $\text{Cl}\cdots\text{O}\cdots\text{Cl}$ angles have values between 86.5 and 93.5° , close to those expected for an octahedral configuration. The IR spectrum shows a strong band at 575 cm^{-1} , attributable to the asymmetric vibration (F_2 mode) of the $\{\text{Cu}_4(\mu_4\text{-O})\}^{6+}$ unit.

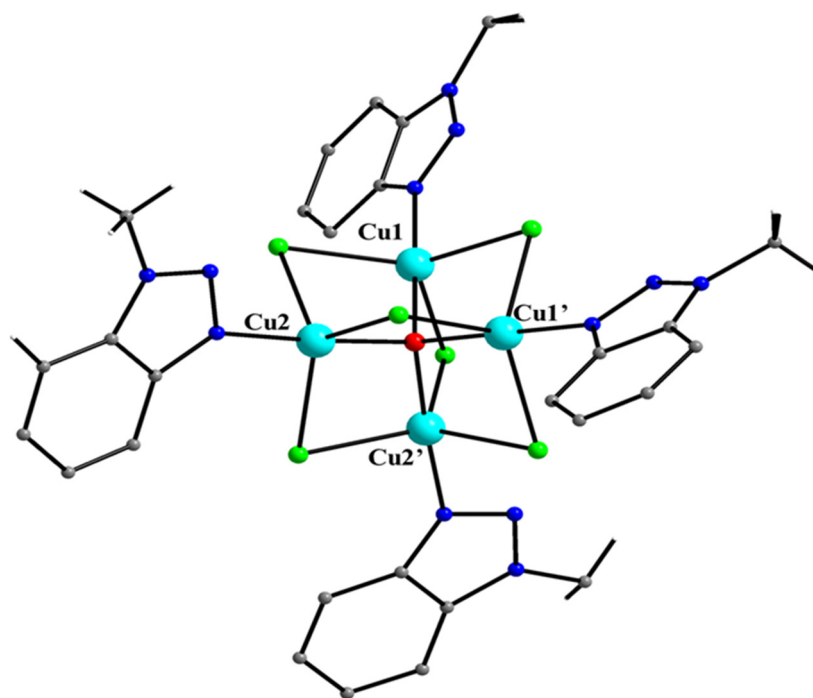


Figure 25. The molecular structure of **20**.

The two Cu^{II} ions in the centrosymmetric cation $[\text{Cu}_2\text{Cl}_2(\text{Mebta})_6]^{2+}$ of **21** (Figure 26) are asymmetrically bridged by two chloro groups; three monodentate Mebta ligands complete five-coordination at each metal. The five donor atoms do not define a regular polyhedron around copper, and the coordination geometry can be described as either square pyramidal or trigonal bipyramidal. The cation of **21** is somewhat structurally similar to the molecule of **17**, the terminal chloro ligands of the latter having been replaced by monodentate Mebta molecules in the former. Complex **21** exhibits a very similar magnetic behavior to that of **17**.

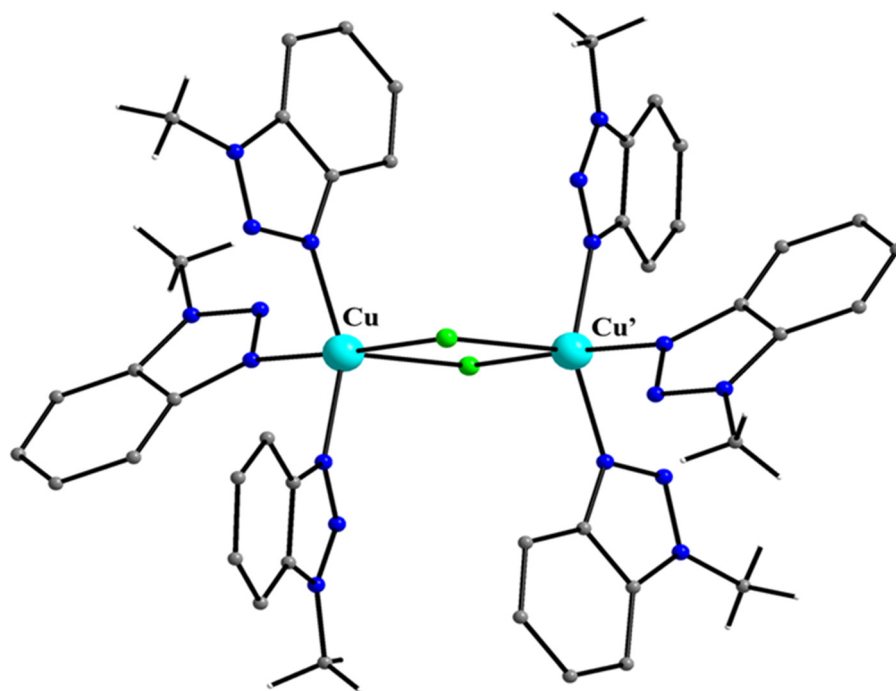
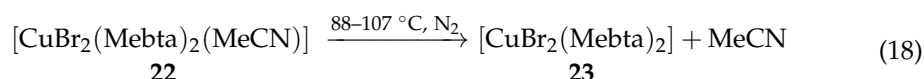


Figure 26. The molecular structure of the cation $[\text{Cu}_2\text{Cl}_2(\text{Mebta})_6]^{2+}$ that exists in the crystal structure of its perchlorate salt **21**.

Mainly for comparison reasons, a systematic investigation of the $\text{CuBr}_2/\text{Mebta}$ reaction system was described [90]. Particular emphasis was placed on determining the influence of the $\text{Mebta}:\text{Cu}^{\text{II}}$ ratio and the nature of the solvent on the identity of the products. Complex $[\text{CuBr}_2(\text{Mebta})_2(\text{MeCN})]$ (**22**) was readily prepared by the 4:1, 3:1 and 2:1 Mebta to Cu^{II} reactions in MeCN in a very good yield (~75%). The 8:1, 6:1, 4:1 and 2:1 reactions in MeOH or EtOH at room temperature gave a brown solution from which was crystallized $[\text{CuBr}_2(\text{Mebta})_2]$ (**23**), also in good yield. Complex **23** was also isolated in pure form from the solid-state endothermic reaction represented by Equation (18). The H_2O concentration in the alcoholic reaction mixtures at high $\text{Mebta}:\text{Cu}^{\text{II}}$ molar ratios gives a different product. Employing ca. 3 M H_2O concentration in MeOH (or EtOH 96%) and 8:1, 5:1 or 3.6:1 $\text{Mebta}:\text{Cu}^{\text{II}}$ ratios, a mixture of light green crystals of $[\text{CuBr}_2(\text{Mebta})_3]$ (**24**) and **23** was obtained.



The five donor atoms in the mononuclear complex **22** (Figure 27) do not define a regular coordination polyhedron around Cu^{II} . However, it can be described as a very distorted trigonal bipyramid with two Mebta N3 atoms at the axial positions; the equatorial bond angles are 142, 114 and 104° . The linear MeCN group binds in a significantly nonlinear fashion ($\text{Cu}-\text{N}\equiv\text{C} = 149^\circ$).

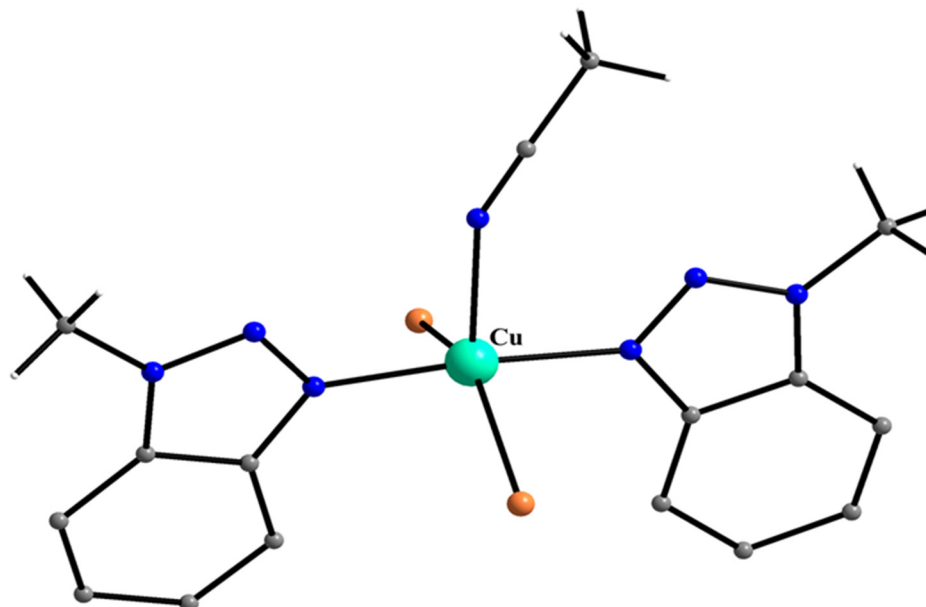


Figure 27. The molecular structure of **22**.

The geometry around the metal ion in the mononuclear complex **23** (Figure 28) can be described as tetrahedrally distorted *trans*-square planar. The *cis* (92.6 and 95°) and *trans* (143.1 and 154.6°) donor atom- Cu^{II} -donor atom angles are intermediate between the expected values for tetrahedral and square planar coordination, respectively. Complex **23** is isomorphous with its chloro counterpart **18**.

The asymmetric unit of **24** contains two structurally similar, but crystallographically independent five-coordinate molecules $[\text{CuBr}_2(\text{Mebta})_3]$; one of them is shown in Figure 29. The coordination sphere of Cu^{II} is composed of two terminal bromo ligands and three N(3)-coordinated Mebta molecules. The coordination geometry is described as distorted trigonal bipyramidal, in which the equatorial plane consists of two bromo ligands and the N atom of a Mebta ligand. Thus, the structure of **24** can be considered as being derived from that of **22** with the replacement of the MeCN ligand of the latter by one Mebta molecule.

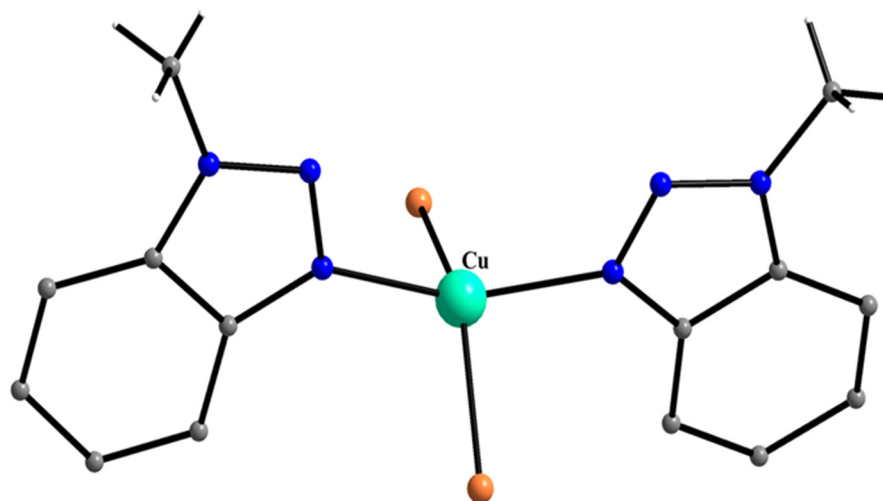


Figure 28. The molecular structure of 23.

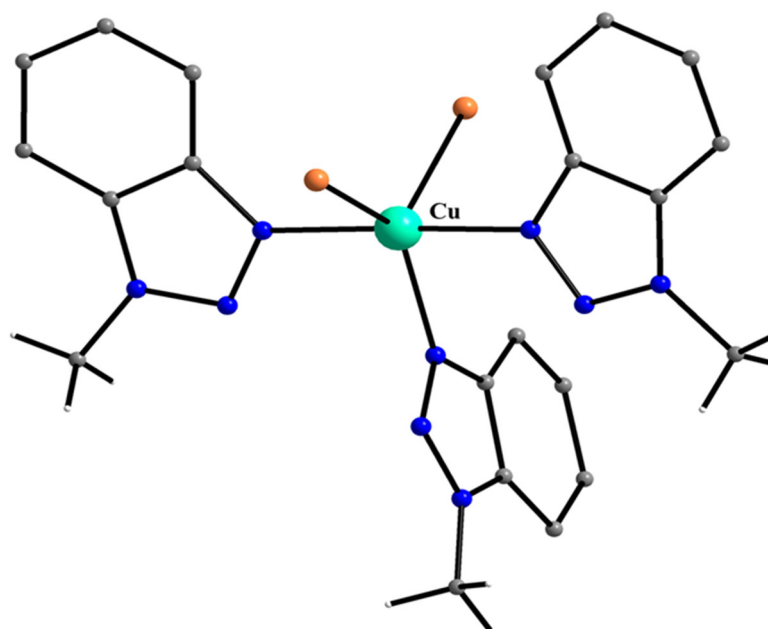


Figure 29. The molecular structure of one of the two crystallographically independent $[\text{CuBr}_2(\text{Mebta})_3]$ molecules that exist in the crystal structure of 24.

Although we do not claim that the synthetic investigation of the $\text{CuX}_2/\text{Mebta}$ ($\text{X} = \text{Cl}, \text{Br}$) reaction systems was complete, evidently, (a) for compounds $[\text{CuX}_2(\text{Mebta})_2]$ (18, 23), the molecular structures remain unchanged upon halide substitution, (b) complexes 17, 19 and 20 have no counterparts in $\text{CuBr}_2/\text{Mebta}$ chemistry, and (c) the 1:3 bromo complex 24 does not have its analogue in $\text{CuCl}_2/\text{Mebta}$ chemistry. Electronic factors may be responsible for (b) and (c).

The extension of the work that led to the 1D compounds 3 and 4 in Cu(II) chemistry gave compound $[\{\text{Cu}\{\text{N}(\text{CN})_2\}_2(\text{Mebta})_2\}]_n$ (25) [81] in typical yields of ~40%. This complex (Figure 30) is isomorphous with 3 (Figure 9) and 4. This intrachain $\text{Cu}^{\text{II}} \cdots \text{Cu}^{\text{II}}$ distance is ~7.34 Å. The crystal structure consists of interdigitated linear chains, where each Mebta ligand lies between two Mebta ligands of an adjacent chain. The centroid-centroid distance between close Mebta molecules belonging to neighboring chains is at the high limit of π - π stacking interactions (~3.80 Å). The complex shows a somewhat unusual, almost linear decrease of the χ_{MT} product from $0.38 \text{ cm}^3 \text{ K mol}^{-1}$ (1.52 B.M.) at 4.2 K. This behavior could not be modeled by a chain model.

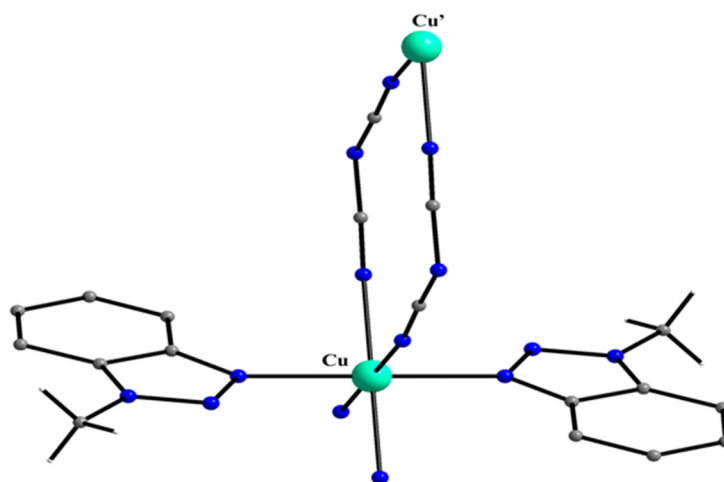


Figure 30. A view of **25** emphasizing the coordination sphere of an Cu^{II} atom in the linear chain.

Attempts to increase the dimensionality of **25** (1D \rightarrow 2D or 3D) were made by using the tricyanomethanide, $\text{C}(\text{CN})_3^-$, ion. Complex $\{[\text{Cu}\{\text{C}(\text{CN})_3\}(\text{Mebta})_2]\}_n$ (**26**) was isolated in a low yield ($\leq 30\%$) through the reaction represented by Equation (19) [81]. However, just as observed in **25**, the $\text{C}(\text{CN})_3^-$ ions bridge via only two of the three available nitrile N atoms, resulting in a 1D linear chain, analogous to those observed in **3**, **4** and **25** (Figure 31). Thus, this ion behaves as a $\mu(1,5)$ ($2.1_1 1_5 0_3$) ligand. Each metal ion is located at a crystallographically imposed inversion center and exhibits a distorted octahedral coordination geometry; the $\text{Cu}^{\text{II}} \cdots \text{Cu}^{\text{II}}$ distance is $\sim 7.25 \text{ \AA}$. The linear chains are packed in an interdigitated manner and the Mebta ligands of neighboring chains are $\sim 3.72 \text{ \AA}$ apart. There is a very weak, antiferromagnetic intrachain $\text{Cu}^{\text{II}} \cdots \text{Cu}^{\text{II}}$ interaction, typical of $\mu(1,5)$ $\text{C}(\text{CN})_3^-$ ligands. This tiny exchange implies essentially zero coupling (non-interacting Cu^{II} atoms), which can be explained by the fact that the unpaired spin on each Cu^{II} center is in a $d_{x^2-y^2}$ orbital, at 90° to the chain direction. The small decrease in $\chi_{\text{M}}T$ below 5 K could also be due to Zeeman-level depopulation effects in the 1 T field used for the measurements.

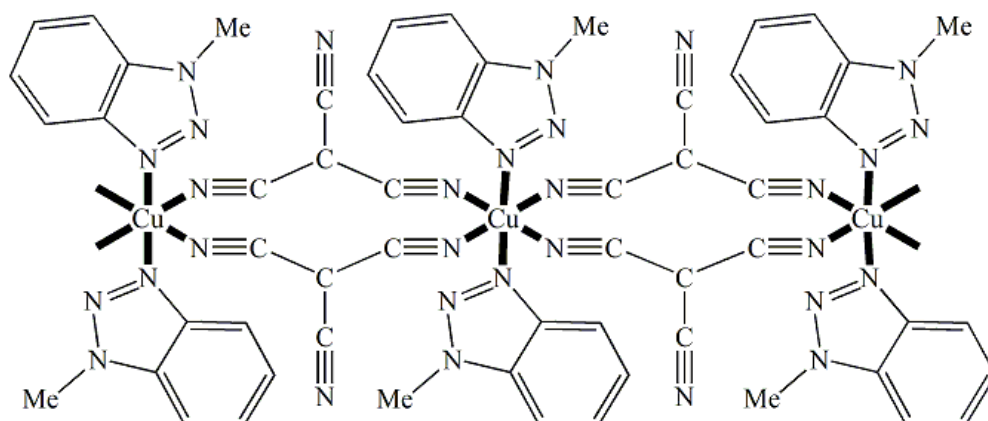
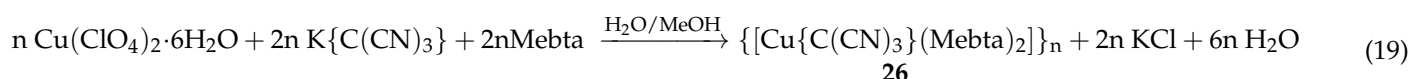


Figure 31. Schematic illustration of a small portion of one linear chain that is present in the crystal structure of **26**.

The azido group is a versatile ligand in coordination chemistry. It can coordinate to up four metal ions when acting as a monoatomic bridge (end-on, EO). The coordination of both terminal N atoms (EE) often leads to coordination polymers. The relatively rare EO/EE combination is capable of bridging up to six metal ions resulting in molecular

clusters or polymeric compounds with aesthetically beautiful structures and interesting properties (mainly magnetic). The 1:2:4 reaction of $\text{Cu}(\text{ClO}_4)_2 \cdot 6\text{H}_2\text{O}$, NaN_3 and Mebta in DMF gave a dark olive-green solution, from which crystals of $\{[\text{Cu}(\text{N}_3)_2(\text{Mebta})]\}_n$ (**27**) were obtained in 35% yield [91]. The same compound can also be isolated using other Cu(II) starting materials, e.g., $\text{CuCl}_2 \cdot 2\text{H}_2\text{O}$, $\text{Cu}(\text{NO}_3)_2 \cdot 3\text{H}_2\text{O}$ and $\text{Cu}(\text{O}_3\text{SCF}_3)_2$. The 1:2:1 stoichiometric reaction did not give the expected complex **27**, but instead the Mebta-free 2D coordination polymer $\{[\text{Cu}_3(\text{N}_6)_6(\text{DMF})_2]\}_n$ built by EO azido groups. It is likely that there is competition between DMF and Mebta for Cu^{II} binding sites. When the organic N_3^- -containing reagent $\text{Me}_3\text{Si}(\text{N}_3)$ was used, the 3D coordination polymer $\{[\text{Cu}(\text{N}_3)_2]\}_n$ was isolated in 40–60% yields depending on the Cu(II) source.

Complex **27** is a 1D coordination polymer. It can be described as consisting of two azido-linked, parallel linear chains (Figure 32). The bridging between the Cu^{II} atoms within each chain is achieved through two μ -(1,1) (or 2.20) EO N_3^- groups; one of these azido groups becomes μ_3 -(1,1,1) (or 3.30) EO and links the metal ions of two neighboring chains giving rise to a 1D corrugated tape. Peripheral ligation about each Cu^{II} is provided by a N(3)-coordinated monodentate Mebta ligand. Thus, the highly elongated, octahedral coordination sphere of each metal ion is $\{\text{Cu}^{\text{II}}\text{N}_5\text{N}'\}$, the five N atoms provided by five azido groups and the N' atom originated from Mebta. The $\text{Cu}^{\text{II}} \cdots \text{Cu}^{\text{II}}$ distance within each chain is 3.63 Å, and these separations between the neighboring parallel chains are 3.10 and 3.60 Å. The Mebta ligands are intramolecularly stacked in an onset, parallel manner; the centroid \cdots centroid distance between adjacent coordinated Mebta molecules is 3.63 Å. The packing of **27** shows the presence of very weak intermolecular interactions between neighboring double chains through π - π stacking forces between the phenyl groups of Mebta.

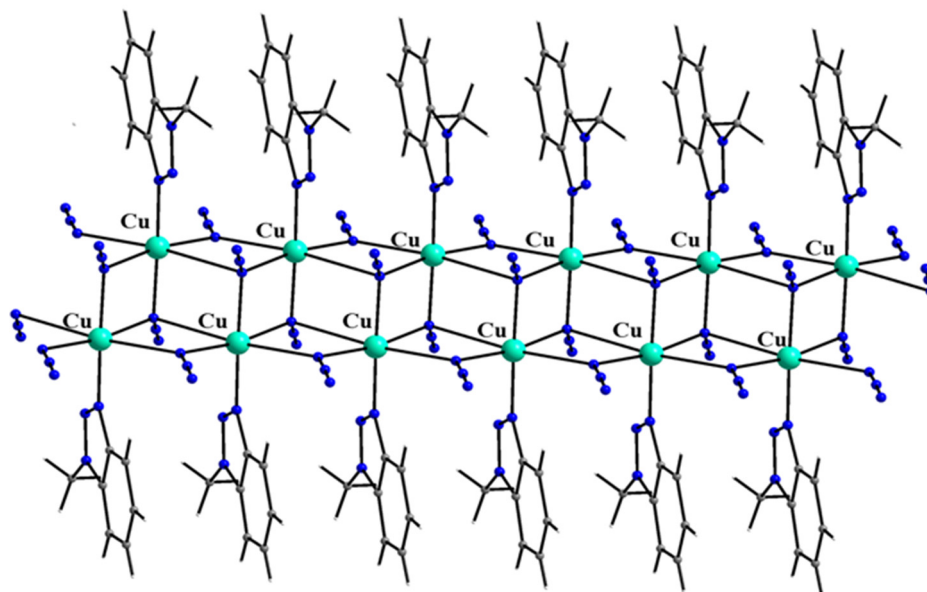
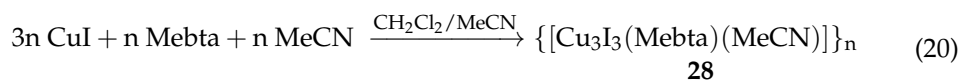


Figure 32. A small portion of one double chain of **27**.

5.8. A Luminescent Copper(I) Polymer with a Unique Bridging Mode of Mebta

The up-to-now described metal complexes of Mebta contain the N(3)-coordinated ligand (1.13010₂; Figure 7, left). The coordination polymer $\{[\text{Cu}^{\text{I}}_3\text{I}_3(\text{Mebta})(\text{MeCN})]\}_n$ (**28**) [80] is unique because the molecule behaves as a bidentate bridging ligand (2.12130₁; Figure 7, right). The reaction of CuI with an excess of Mebta in CH_2Cl_2 at room temperature for 24 h caused the precipitation of a yellow solid, recrystallization of which from MeCN

gave light green crystals of the product, Equation (20). The reaction probably proceeds through the attack of MeCN on the intermediate $\{[\text{Cu}^{\text{I}}_2\text{I}_2(\text{Mebta})]\}_n$ (**29**) [92].



The asymmetric unit of **28**, illustrated in Figure 33, contains three crystallographically independent Cu^{I} atoms, one bidentate bridging Mebta group and one terminal MeCN molecule [80]. The three iodo ligands are μ_3 , in such a manner that each iodide is at the apex and the three metal centers at the corner of the base of a trigonal pyramid. The Mebta ligand bridges Cu1 and Cu2, while the MeCN molecule completes the coordination sphere of Cu3. The coordination geometries are trigonal pyramidal for Cu1 and Cu2 and tetrahedral for Cu3. Thus, the complex consists of zigzag chains being a 1D coordination polymer. The chains are interconnected through π - π stacking interactions generating a 2D network. Solid **28** exhibited green light emission upon excitation with wavelengths below 475 nm, with a lifetime of 47 μs ; the photophysical behavior was further elaborated using DFT calculations.

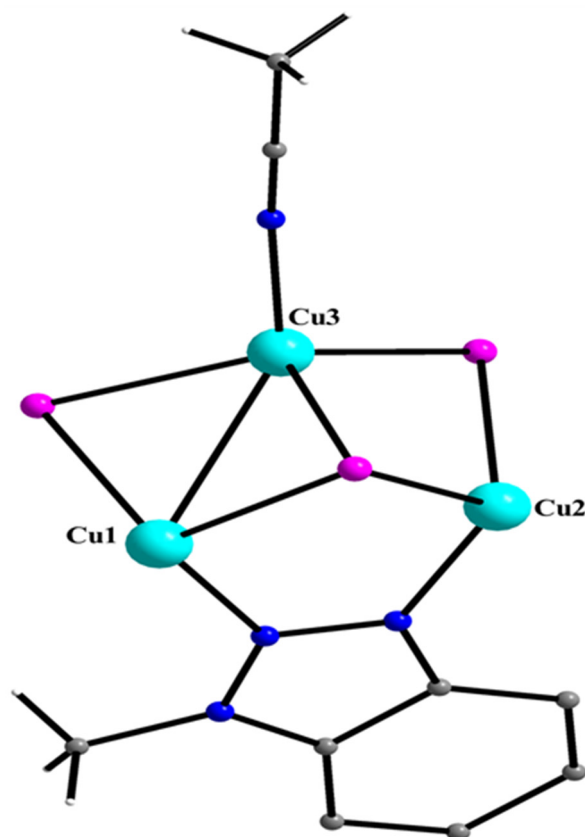


Figure 33. The asymmetric unit of the 1D polymer **28**.

The single crystal X-ray data set for **29** was poor, but a tentative/preliminary structural solution gave the polymeric double-stranded stairlike ribbon motif shown in Figure 34. It is worth mentioning that the reaction solution that led to the isolation of **29** did not contain Mebta! The complex was formed as a byproduct from the 1:1:1 reaction of CuI, KI and benzotriazole (btaH; Figure 1, left) in MeOH under solvothermal conditions (140 °C, 72 h). The main product [92] was the 3D ionic polymer $\{(\text{Me}_2\text{bta})_4[(\text{Cu}_{10}\text{I}_{10})(\text{Cu}_6\text{I}_6)(\text{Cu}(\text{bta})_2)]_3\text{I}^- \cdot 1.5\text{I}_2\}_n$, where $(\text{Me}_2\text{bta})^+$ is the 1,3-dimethyl-1,2,3-benzotriazolium cation (Figure 6).

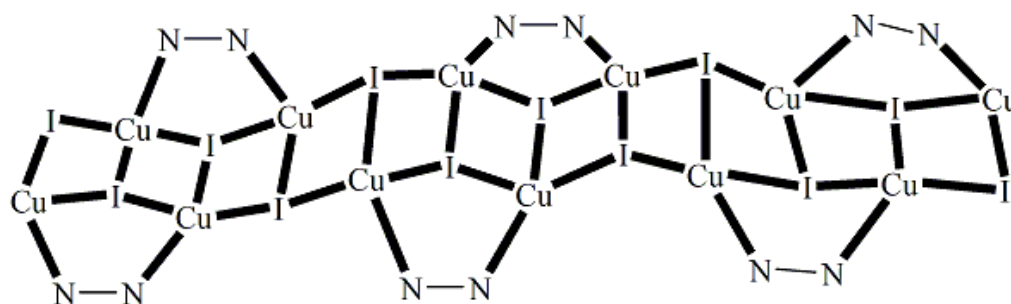
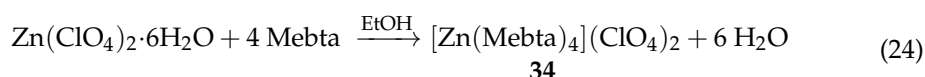
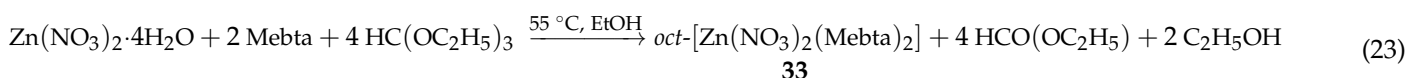
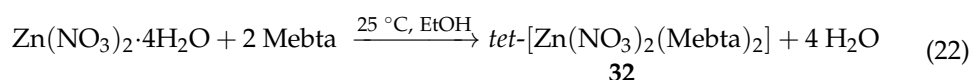
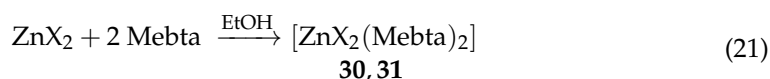


Figure 34. A small part of a 1D chain containing corrugated double-stranded stairlike $\{CuI\}_n$ chain; this model was derived from a poor structural solution of **29**. N-N represents the N(2)-N(3) part of Mebta that contains the two donor atoms of the Mebta ligands (the whole ligands are not drawn for clarity reasons). The Cu^I atoms are tetrahedral, with a coordination sphere comprising three iodo groups and one N atom of a bidentate bridging ligand. The terminal Cu^{II} atoms appear as three-coordinate, but they are actually four-coordinate.

5.9. Filling in the Empty Position of Zn(II)

In an attempt to fill in the empty Zn(II) position in the “Periodic Table” of Mebta, complexes $[ZnBr_2(Mebta)_2]$ (**30**), $[ZnI_2(Mebta)_2]$ (**31**), *tet*- $[Zn(NO_3)_2(Mebta)_2]$ (**32**), *oct*- $[Zn(NO_3)_2(Mebta)_2]$ (**33**) and $[Zn(Mebta)_4](ClO_4)_2$ (**34**) were prepared and structurally characterized [3]. The preparation of the compounds is summarized in Equations (21)–(24) (X = Br, I).



Complexes **30** and **31** were obtained in moderate yields. Changes in the reaction ratio from 1:2 to 1:1 or 1:4 and the solvent from EtOH or MeCN led again to **30** and **31**, suggesting that the 1:2 complexes are thermodynamically favored under the conditions employed. Like $Ni(NO_3)_2 \cdot 6H_2O$ /Mebta (part 5.5), the 1:2 $Zn(NO_3)_2 \cdot 4H_2O$ /Mebta reaction system is sensitive to the H_2O concentration but in a different manner. The 1:2 reaction of $Zn(NO_3)_2 \cdot 4H_2O$ and Mebta at room temperature gave compound *tet*- $[Zn(NO_3)_2(Mebta)_2]$ (**32**) in a ca. 50% yield, where “tet” denotes a tetrahedral geometry at the metal ion. The analogous reaction at 55 °C in the presence of an excess of the dehydrating agent TEOF (part 5.5) gave compound *oct*- $[Zn(NO_3)_2(Mebta)_2]$ (**33**) in a ca. 60% yield. The abbreviation “oct” denotes an octahedral coordination sphere. It was hypothesized that in the presence of H_2O contained in zinc(II) nitrate and in EtOH, the octahedral species $[Zn(NO_3)_2(Mebta)_2(H_2O)_2]$ (with monodentate nitrates) is formed in solution and the aqua ligands are removed during crystallization retaining the monodentate character of nitrates and leading to the tetrahedral complex **32**. When H_2O is practically absent (use of TEOF under heating), the octahedral species $[Zn(NO_3)_2(Mebta)_2]$ (with bidentate nitrato groups) is formed in solution and this is precipitated yielding **33**. The use of ClO_4^- ions, which have little tendency for coordination, led to the cation complex **34** in a 45% yield.

Complexes **30** and **31** (Figure 35) are isostructural, but not isomorphous. The Zn^{II} atom is coordinated by two halo groups and two N atoms from two N(3)-coordinated monodentate Mebta ligands. In the tetrahedral molecules, the donor atom- Zn^{II} -donor

atom bond angles are in the ranges 104–116° for **30** and 104–115° for **31**. The Br-Zn^{II}-Br and I-Zn^{II}-I angles are the largest; inter ligand repulsions between the large and negatively charged halides seem to be responsible for this and the observed distortion from the regular tetrahedral coordination.

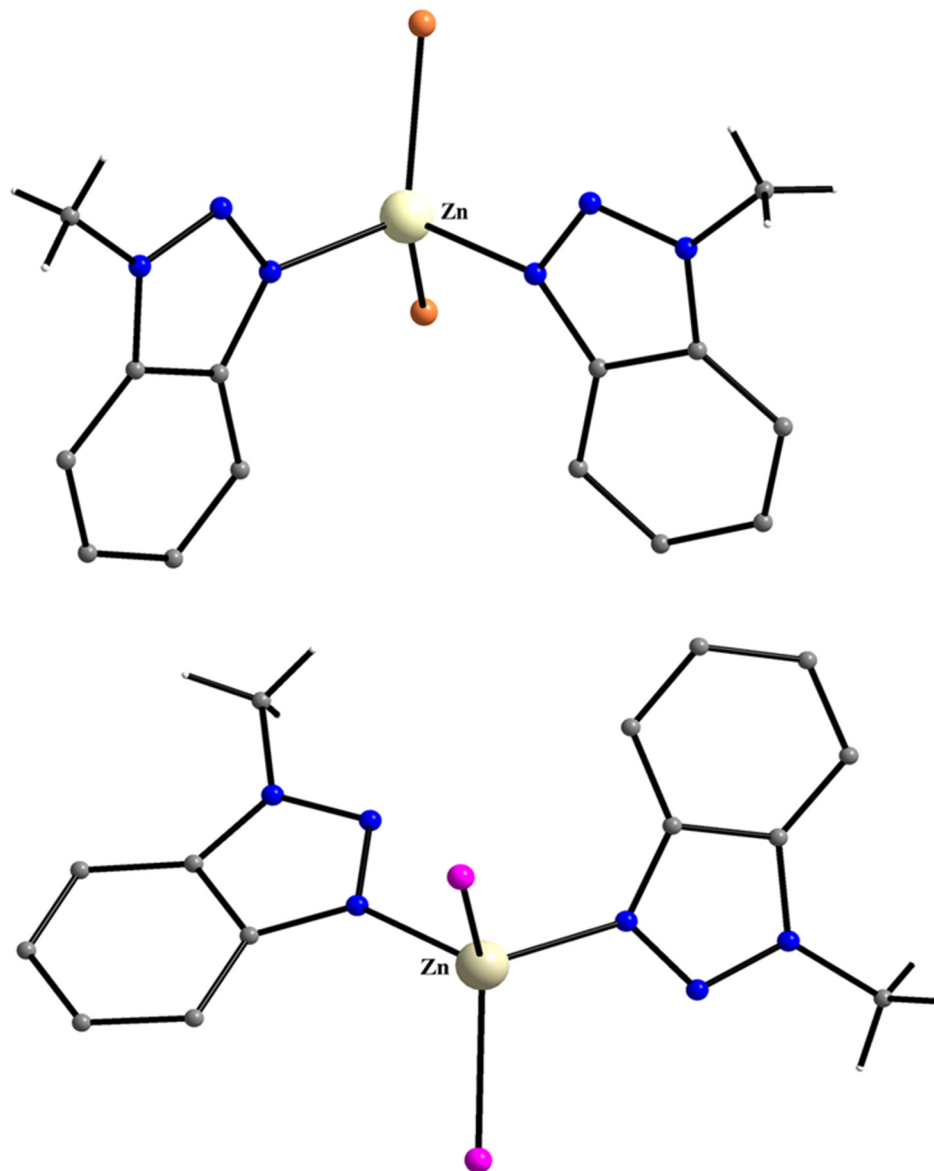


Figure 35. The molecular structures of **30** (up) and **31** (bottom).

The Zn^{II} atom in *tet*-[Zn(NO₃)₂(Mebta)₂] (**32**) (Figure 36, up) is bonded to two monodentate Mebta ligands and two (practically) monodentate groups. The coordination geometry at the metal center is very distorted tetrahedral with the angles around Zn^{II} being in the range 88–118°. Complex *oct*-[Zn(NO₃)₂(Mebta)₂] (**33**) (Figure 36, bottom) is isomorphous with its Co(II) (**10**) and Ni(II) (**12**) analogues (*vide supra*). The metal ion sits on a crystallographic C₂ axis which bisects the N_{Mebta}-Zn^{II}-N_{Mebta} angle. The significant distortion of the octahedral stereochemistry is a consequence of the small bite angles (57°) of the bidentate chelating nitrato groups. The Zn^{II}-O_{nitrato} bonds *trans* to N_{Mebta} (2.39 Å) are longer than those *trans* to O (2.06 Å). As expected, the O-N-O angle involving the coordinated nitrato oxygen is the smallest (116°) of the three O-N-O angles. The Zn^{II}-N bond lengths in **33** are longer than the corresponding ones in **32**, due to the higher coordination number of Zn^{II} in the former than in the latter (6 vs. 4).

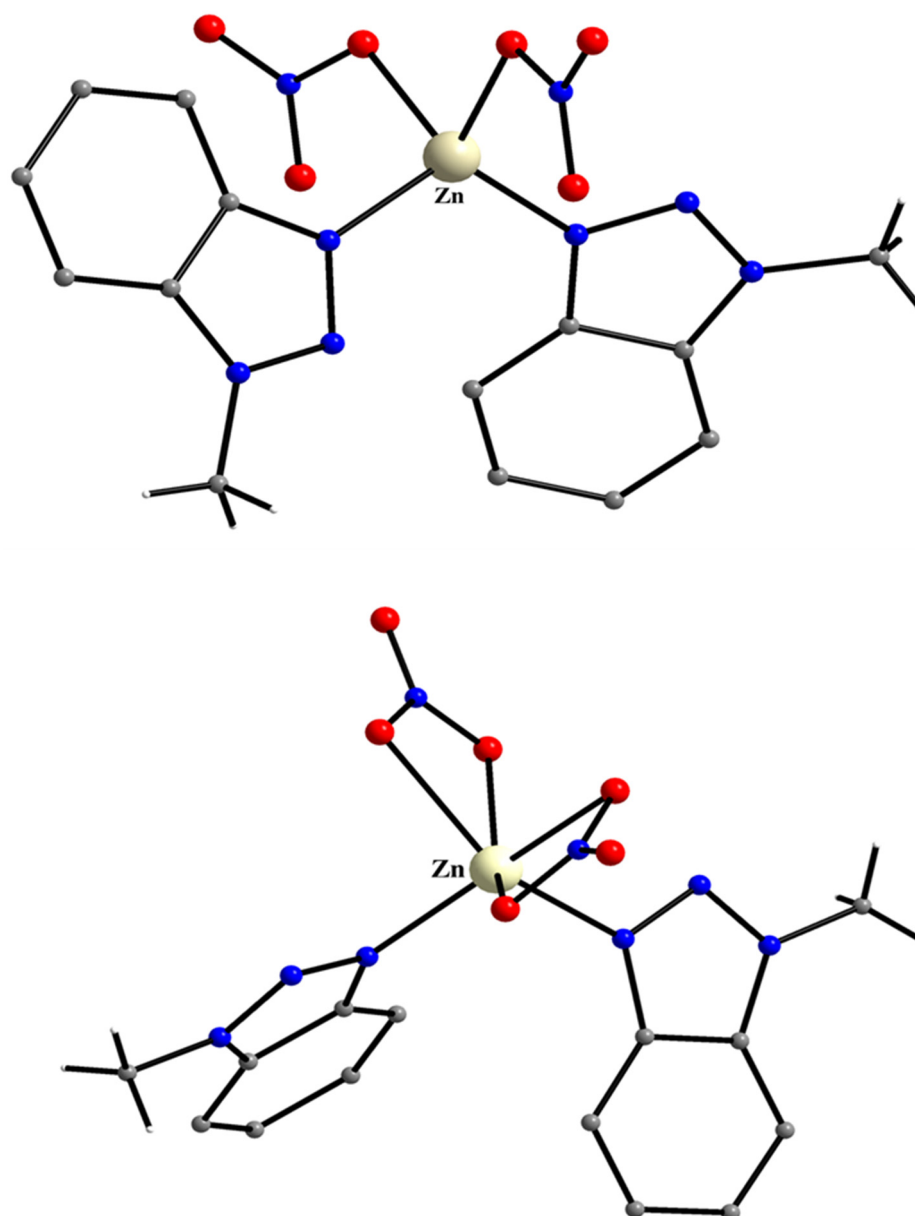


Figure 36. The molecular structures of **32** (up) and **33** (bottom).

In the cation of **34** (Figure 37), the Zn^{II} atom is coordinated to four monodentate Mebta ligands in a tetrahedral manner; the six N–Zn–N angles range between 108 and 111°. The ClO_4^- counterions are also tetrahedral.

A combination of π – π stacking interactions and non-classical H bonds gives rise to beautiful 3D architectures in the crystal structures of **30–34**.

The molar conductivity value (Λ_{M}) of **34** in DMSO (25 °C) is 71 $\text{S cm}^2 \text{mol}^{-1}$ suggesting a 1:2 electrolyte [93], as expected from its ionic structure. Somewhat to our surprise, the Λ_{M} values of **30–33** (70–80 $\text{S cm}^2 \text{mol}^{-1}$) in the same solvent are also indicative of 1:2 electrolytes despite the fact that the compounds are neutral in the solid state! This is strong evidence for the decomposition of the complexes in solution, most probably through the reaction represented by Equation (25), where $\text{X} = \text{Br}, \text{I}, \text{NO}_3$. In agreement with the proposal, the Λ_{M} values of these complexes in MeNO_2 (a solvent with weak capacity for coordination) are between 10 and 15 $\text{S cm}^2 \text{mol}^{-1}$, values indicative of essentially non-electrolytes [93]. The validity of Equation (25) is further corroborated by the fact that the ^1H NMR [3,38,39,42,75,76] and $^{13}\text{C}\{^1\text{H}\}$ NMR [3,38,42,75–77] spectra of the complexes in d_6 -DMSO are identical with those of the free Mebta in the same solvent.

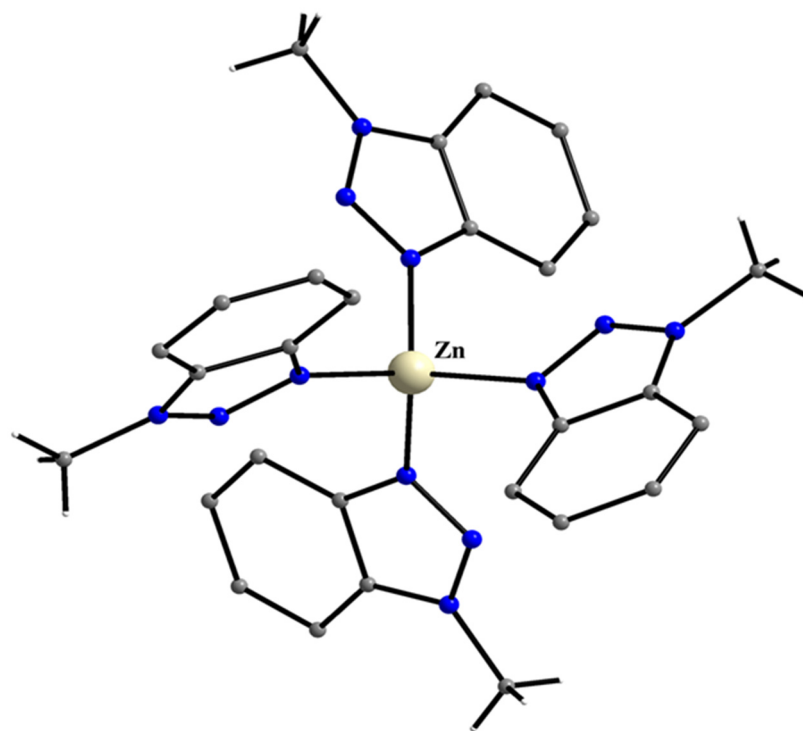
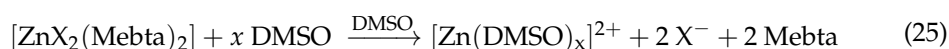


Figure 37. The molecular structure of the cation $[\text{Zn}(\text{Mebta})_4]^{2+}$ that is present in the crystal structure of complex **34**.



5.10. A Two-Coordinate Au(I) Complex

Cross-coupling reactions for the synthesis of useful organic compounds catalyzed by transition-metal complexes are important in organic chemistry. Conjugated 1,3-diynes and polyynes are useful because they are often found in substances with biological activities and natural products. Complex $[\text{Au}(\text{Ph}_3\text{P})(\text{Mebta})](\text{OTf})$ (**35**), where TfO^- is the trifluoromethanesulfonate anion, was crystallized during systematic efforts for its use as a homogeneous catalyst for the synthesis of unsymmetrical 1,3-butadiynes from terminal alkynes and hypervalent iodine(III) reagents (Figure 38) [94].

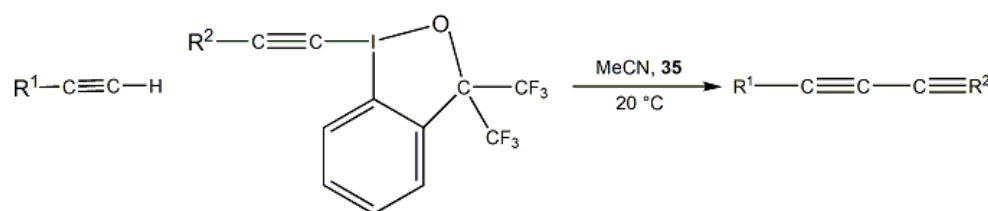


Figure 38. Complex **35**-catalyzed cross-coupling of terminal alkynes with ethynylbenziodioxole hypervalent iodine reagents (R^1, R^2 = various organic groups).

The cation of **35** (Figure 39) consists of a two-coordinate Au^{I} atom with almost linear geometry. The metal ion forms bonds to one triphenylphosphine molecule and one monodentate Mebta ligand.

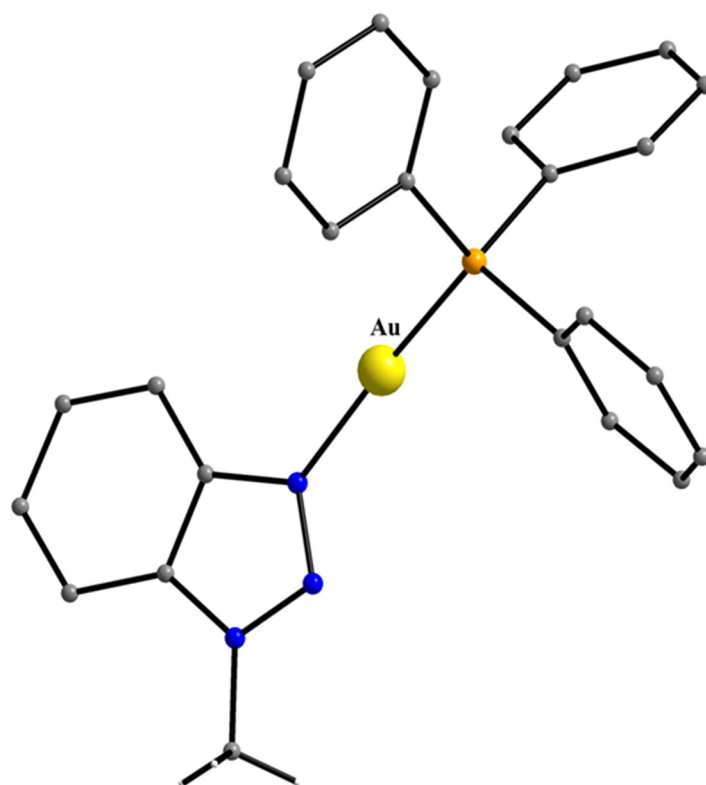


Figure 39. The molecular structure of the cation $[\text{Au}(\text{Ph}_3\text{P})(\text{Mebta})]^+$ that is present in the crystal structure of 35.

5.11. A Hexagonal Bipyramidal $\{\text{U}^{\text{VI}}\text{O}_2\}^{2+}/\text{Mebta}$ Complex

The $\{\text{U}^{\text{VI}}\text{O}_2\}^{2+}/\text{benzotriazole}$ chemistry is currently receiving attention because benzotriazole-decorated graphene oxide can be used for the removal of uranium(VI) in the nuclear industry [21]; see also Section 3. Prior to our work [95], few uranyl/azole complexes had been synthesized, and none was known with benzotriazoles as ligands.

The 1:2 reaction between $\text{UO}_2(\text{NO}_3)_2 \cdot 6\text{H}_2\text{O}$ and Mebta in MeCN at room temperature gave a yellowish green solution, that upon storage at 20 °C produced crystals of $[\text{UO}_2(\text{NO}_3)_2(\text{Mebta})_2]$ (36) of the same color in 40% yield. The U^{VI} atom is at a crystallographically imposed inversion center. The metal is surrounded by two N and six O atoms in a hexagonal bipyramidal coordination environment. The two uranyl oxygen atoms occupy the axial positions. The four O atoms are from two bidentate chelating nitrato groups and the two N atoms are from two monodentate Mebta ligands; these six atoms are located in the almost planar equatorial plane. In the complex, the benzene rings are at the opposite side of the molecule. The dihedral angle between the planes of Mebta and the planes of the coordinate nitrato groups is 87°. The molecular structure of 36 is shown in Figure 40. H bonds and π - π stacking interactions stabilize the crystal structure. The IR spectrum of the compound exhibits a strong band at 944 cm^{-1} assigned to the IR-active antisymmetric stretching vibration of the $\{\text{O}=\text{U}=\text{O}\}^{2+}$ moiety (ν_3); this vibration is not visible in the Raman spectrum, in agreement with the centrosymmetric nature of the uranyl group. The Raman-active uranyl symmetric stretch (ν_1) appears at $\sim 860\text{ cm}^{-1}$.

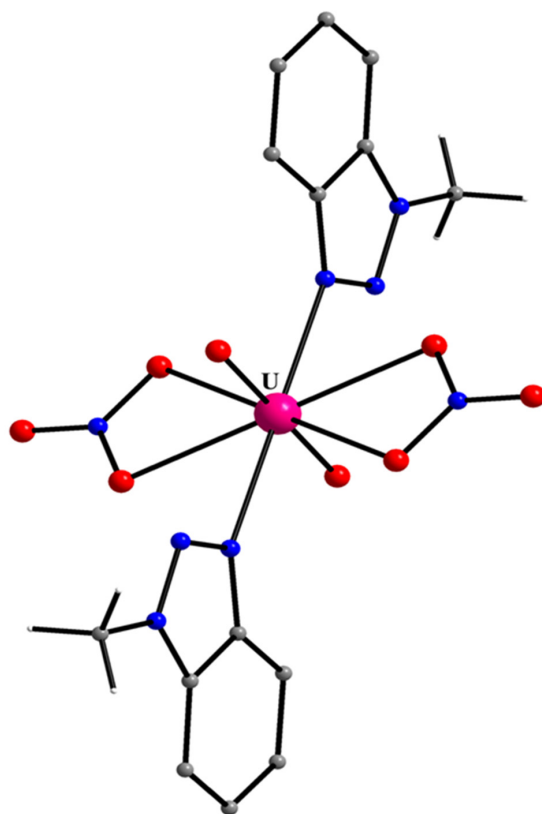


Figure 40. The molecular structure of 36.

6. Unpublished Work on the Coordination Chemistry of Mebta

The research described in Section 5 refers to published work. Our group continues to study the coordination chemistry of Mebta and at the time of writing, there are several unpublished results. In this section, we shall briefly comment on *selected*, structurally characterized metal complexes. All the to-date known such complexes are listed in Table 1, while the molecular structures of some compounds are shown in Figures 41–49.

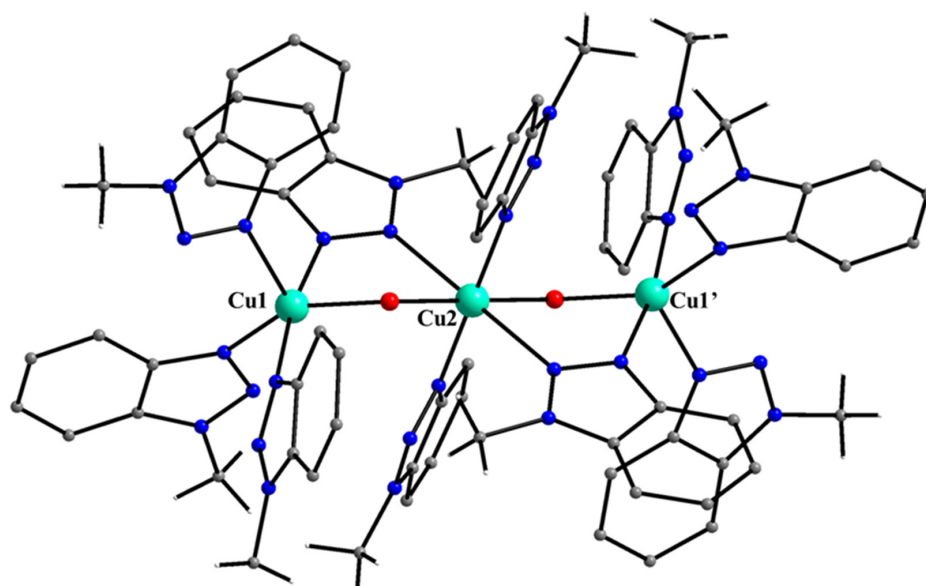


Figure 41. The molecular structure of the cation $[\text{Cu}_3(\text{OH})_2(\text{Mebta})_{10}]^{4+}$ that is present in the crystal structure of 38.

Table 1. Unpublished metal complexes of Mebta from our group.

A Ni(II) Complex
<i>trans</i> -[Ni(SCN) ₂ (MeOH) ₂ (Mebta) ₂] (37) ^a
A Trinuclear Cu(II) Cluster
[Cu ₃ (OH) ₂ (Mebta) ₁₀](BF ₄) ₄ (38)
Polymeric Dicyanoamido Co(II) and Zn(II) Complexes
{[Co{N(CN) ₂ } ₂ (Mebta) ₂]} _n ^b (39)
{[Zn{N(CN) ₂ } ₂ (Mebta) ₂]} _n ^b (40)
A Trinuclear Carboxylato-Bridged Zn(II) Cluster
[Zn ₃ (O ₂ CPh) ₆ (Mebta) ₂] (41)
Three-Coordinate Silver(I) Complexes
[Ag(NO ₃)(Mebta) ₂] (42)
[Ag(CF ₃ SO ₃)(Mebta) ₂] (43)
Cd(II) Complexes
[CdBr ₂ (Mebta) ₂] (44)
[CdI ₂ (Mebta) ₂] (45)
<i>trans</i> -[Cd(NO ₃) ₂ (H ₂ O) ₂ (Mebta) ₂] (46)
{[CdBr ₂ (Mebta)]} _n ^b (47)
{[Cd ₃ (SCN) ₆ (Mebta)(H ₂ O)]} _n ^b (48)
{[Cd _{2.5} (SCN) ₅ (Mebta) ₄ (H ₂ O)]} _n ^b (49)
{[Cd{N(CN) ₂ } ₂ (Mebta) ₂]} _n ^b (50)
Hg(II) Complexes
{[HgCl ₂ (Mebta)]} _n ^b (51)
{[HgBr ₂ (Mebta)]} _n ^b (52)
[Hg ₂ I ₄ (Mebta) ₂] (53)
{[Hg ₂ (SCN) ₄ (Mebta) ₃]} _n ^b (54)
In(III) Complexes
<i>mer</i> -[InCl ₃ (H ₂ O)(Mebta) ₂] (55)
<i>mer</i> -[InBr ₃ (H ₂ O)(Mebta) ₂] (56)
<i>mer</i> -[InCl ₃ (H ₂ O) ₂ (Mebta)] (57)
<i>mer</i> -[In(Cl/Br) ₃ (H ₂ O) ₂ (Mebta)] (58)
[InI ₃ (Mebta) ₂] (59)
Sn(IV) Complexes
[(Me) ₂ SnCl ₂ (Mebta) ₂] (60)
(MebtaH) ₂ [SnCl ₆] ^c (61)
(MebtaH) ₂ [Sn(Cl _{0.55} Br _{0.45}) ₆] ^c (62)
Heterometallic Coordination Polymers
{[HgCo(SCN) ₄ (Mebta) ₂]} _n ^d (63)
{[HgCo(SCN) ₂ Cl ₂ (H ₂ O) ₂ (Mebta) ₂]} _n ^b (64)
{[HgCo(SCN) ₂ Br ₂ (DMF) ₂ (Mebta) ₂]} _n ^b (65)
{[HgNi(SCN) ₂ Cl ₂ (MeOH) ₂ (Mebta) ₂]} _n ^b (66)

^a This complex is a polymorph of **11** (part 5.5). ^b 1D coordination polymers. ^c In these complex salts, the protonated Mebta molecules act as counterions. ^d 3D coordination polymer.

With the exception of the Cu(I) complex **28** [80] (and possibly **29** [92]), where Mebta adopts the bridging ligation mode 2.1₂.1₃0₁ (Figure 7, right), in all the other described metal complexes in Section 5 Mebta behaves as a monodentate ligand coordinating through the N atom of the position 3 of theazole ring (1.1₃0₁0₂; Figure 7, left). The latter had also been predicted [3] through theoretical calculations at the ab initio level (MR2) in ethanolic solution (EtOH is the most often used solvent for the preparation of its metal complexes); see also Section 5. However, the crystal structures of **28** and **29** revealed a contradiction between theory and experiment. In an attempt to “force” the bidentate bridging behavior of Mebta, we performed reactions of Cu(II) starting materials with poorly coordinating anions and Mebta, with the metal ion in excess. Such a reaction between Cu(BF₄)₂·6H₂O and Mebta in EtOH afforded the trinuclear cluster [Cu₃(OH)₂(Mebta)₁₀](BF₄)₄ (**38**) in low to moderate yields, Equation (26). The released protons might be expected to decompose the product by reacting with the hydroxo ligands. As in the case of the dinuclear oxo-bridged Fe(III) complex **5** (part 5.3), it is possible that the protons are neutralized by Mebta which

has not reacted. If this assumption is correct, the stoichiometric reaction can be represented by Equation (27).

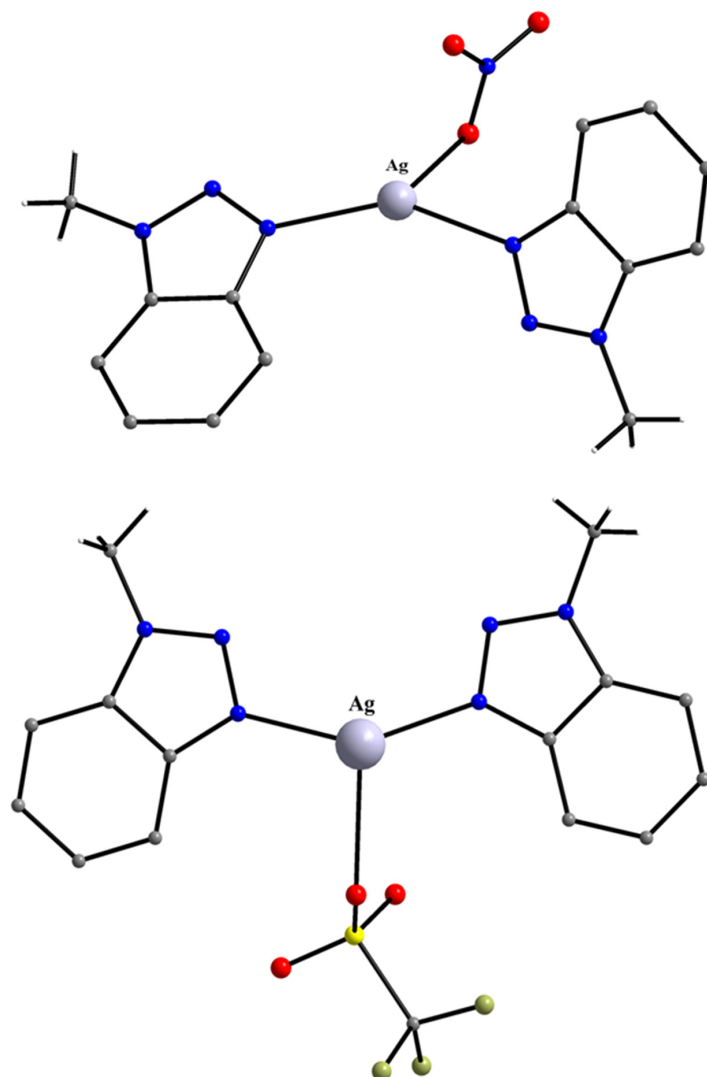


Figure 42. The molecular structures of 42 (up) and 43 (bottom).

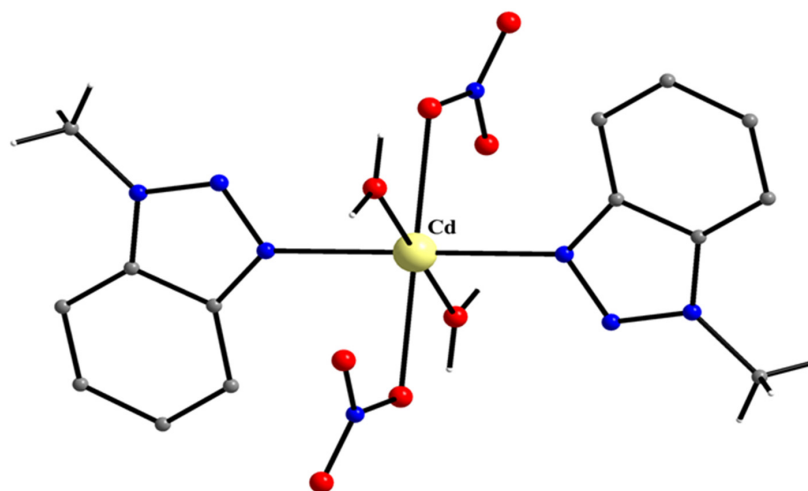


Figure 43. The molecular structure of 46.

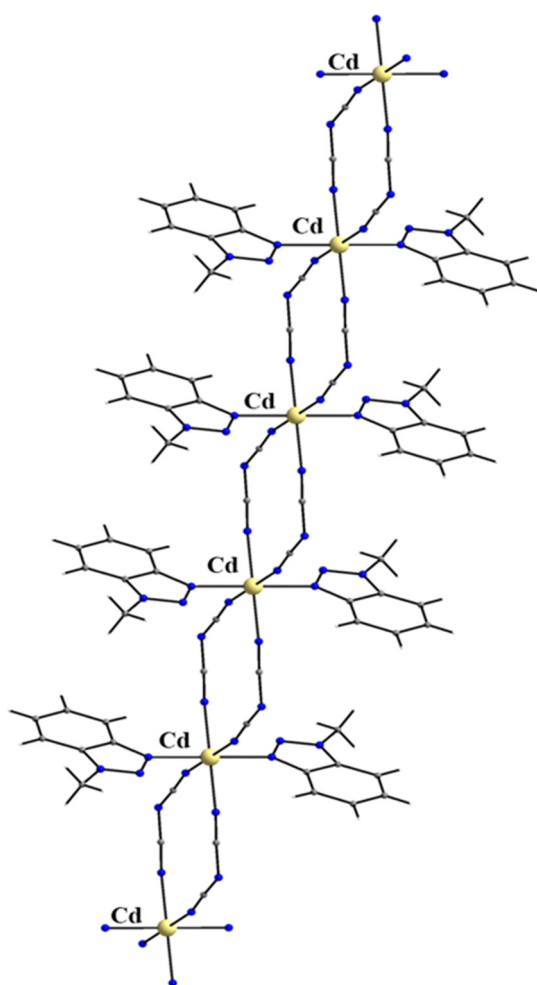


Figure 44. A small portion of one linear chain that is present in the crystal structure of 50.

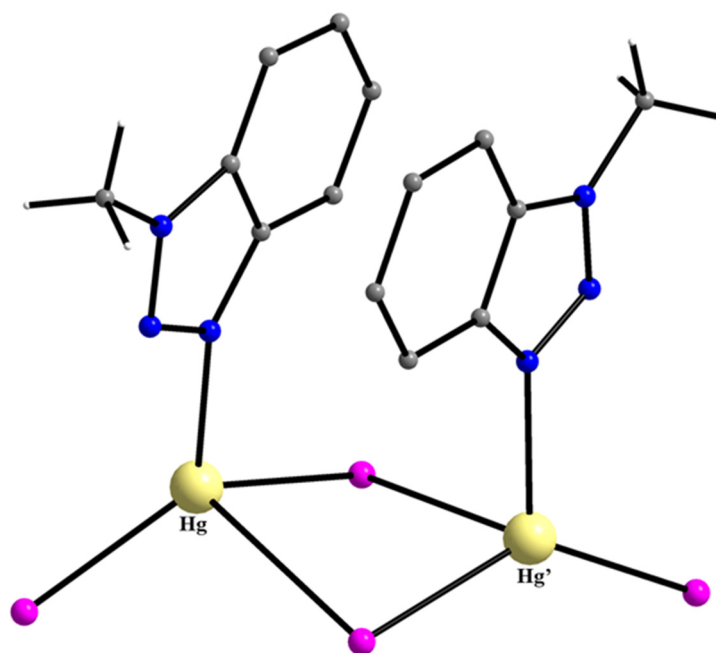


Figure 45. The molecular structure of 53.

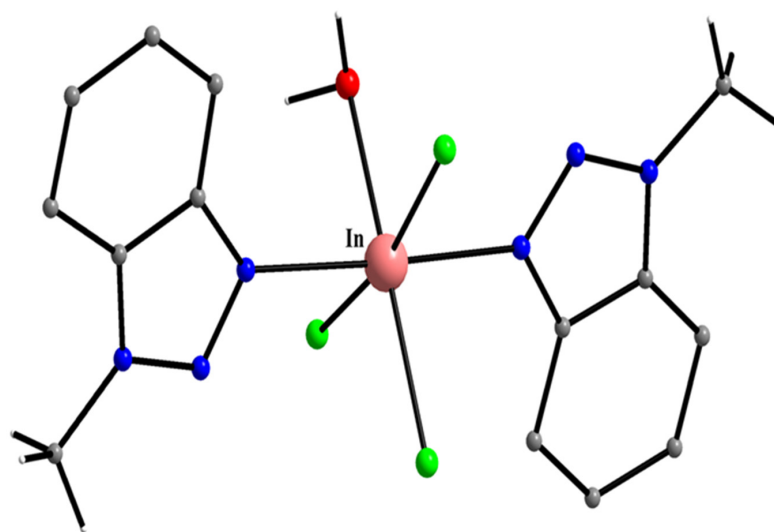


Figure 46. The molecular structure of 55.

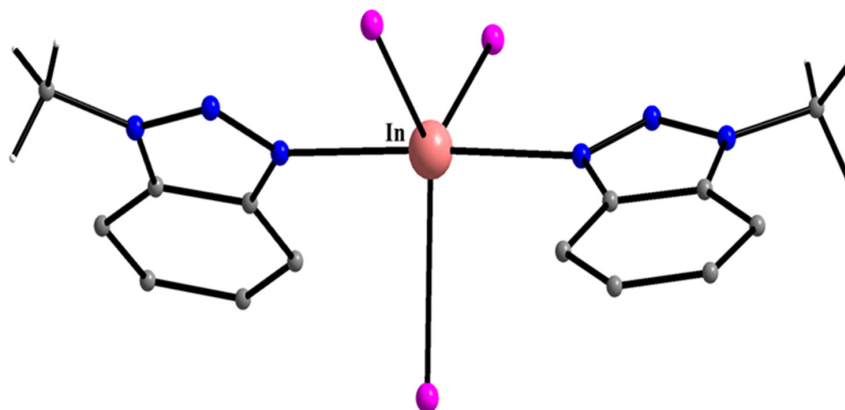


Figure 47. The molecular structure of 59.

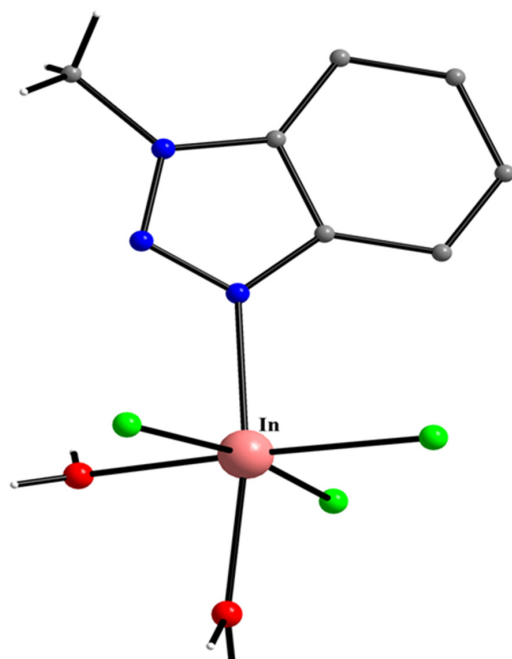


Figure 48. The molecular structure of 57.

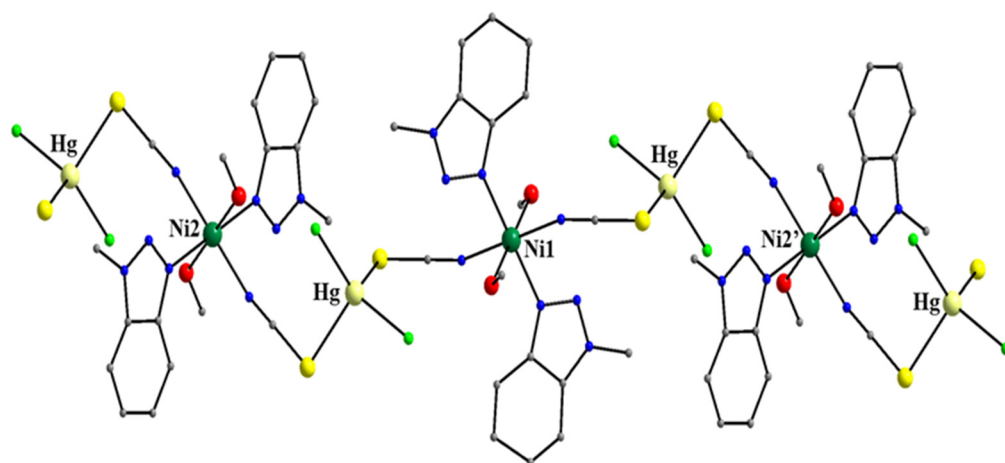
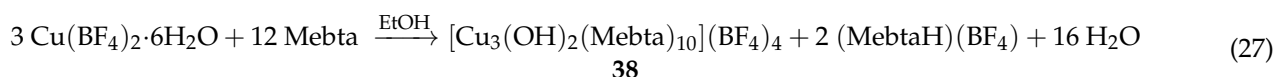
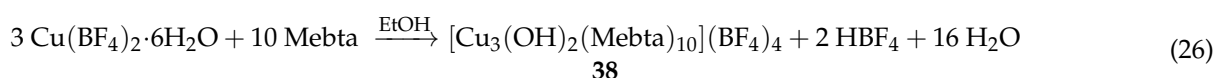


Figure 49. A small portion of one chain that is present in the crystal structure of **66**.



In the centrosymmetric cation $[\text{Cu}_3(\text{OH})_2(\text{Mebta})_{10}]^{4+}$ (Figure 41), the central six-coordinate Cu^{II} atom is doubly bridged to each 5-coordinate metal ion through a hydroxo atom and one 2.1₂1₃0₁ Mebta group. Two monodentate Mebta ligands complete the octahedral coordination sphere of the central copper and three, also monodentate ligands give each terminal copper a coordination number of five.

The silver(I) complexes $[\text{Ag}(\text{NO}_3)(\text{Mebta})_2]$ (**42**) and $[\text{Ag}(\text{CF}_3\text{SO}_3)(\text{Mebta})_2]$ (**43**) contain three monodentate ligands and the Ag^{I} center adopts a trigonal planar coordination geometry (Figure 42). The antimicrobial potency of the complexes, their inorganic starting materials $[\text{AgNO}_3, \text{Ag}(\text{CF}_3\text{SO}_3)]$ and the free organic ligand (Mebta) was evaluated against Gram-negative and Gram-positive microbes. The silver(I) salts exhibit moderate properties, Mebta shows no activity, whereas the complexes exhibit their strongest activity towards the Gram-negative bacterial strain of *P. aeruginosa*.

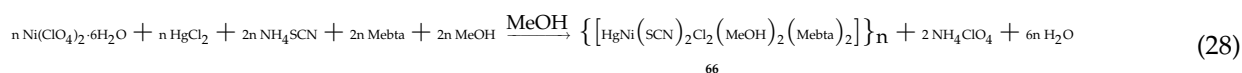
The Cd(II) and Hg(II) chemistry of Mebta is also interesting (Figures 43–45). For example, complex $[\text{Cd}(\text{NO}_3)_2(\text{H}_2\text{O})_2(\text{Mebta})_2]$ (**46**) has an all-*trans* coordination environment, $[\{\text{Cd}\{\text{N}(\text{CN})_2\}_2(\text{Mebta})\}]_n$ (**50**) is a six-coordinate 1D polymer structurally similar to **3** (Figure 9), **4** (part 5.3) and **25** (Figure 30), while $[\text{Hg}_2\text{I}_4(\text{Mebta})_2]$ (**53**) is a doubly iodo-bridged dimer with intramolecular π - π stacking interaction between the two Mebta ligands.

The best solvent for the synthesis and crystallization of In(III)/Mebta complexes was proven to be CHCl_3 . The 1:2 reactions between InX_3 ($\text{X} = \text{Cl}, \text{Br}, \text{I}$) and Mebta in refluxing CHCl_3 gave complexes *mer*- $[\text{InCl}_3(\text{H}_2\text{O})(\text{Mebta})_2]$ (**55**), *mer*- $[\text{InBr}_3(\text{H}_2\text{O})(\text{Mebta})_2]$ (**56**) and *mer*- $[\text{InI}_3(\text{Mebta})_2]$ (**59**) in moderate to good yields. The chloro (Figure 46) and bromo complexes consist of octahedral molecules with the halogeno ligands in *mer* positions. The $[\text{InI}_3(\text{Mebta})_2]$ (**59**) molecules have a trigonal bipyramidal environment around In^{III} with the monodentate N(3)-coordinated Mebta ligands at axial positions (Figure 47).

The results from the 1:1 (and not 1:2 as in **55**, **56** and **59**) reactions of InX_3 ($\text{X} = \text{Br}, \text{I}$) in refluxing CHCl_3 were unexpected and surprising. The reaction of InBr_3 gave complex *mer*- $[\text{In}(\text{Cl}/\text{Br})_3(\text{H}_2\text{O})_2(\text{Mebta})]$ (**58**) with partial Cl^-/Br^- occupancy, and that of InI_3 yielded the all-chloro complex *mer*- $[\text{InCl}_3(\text{H}_2\text{O})_2(\text{Mebta})]$ (**57**); the molecular structure of the latter is shown in Figure 48. The 1:1 metal-to-ligand ratio is retained in the products while the halogeno ligands are again in *mer* positions. The only explanation for the presence of chloro ligands in **57** and **58** is that they have originated from the solvent used (CHCl_3) under

refluxing conditions. Further experimental work and ab initio calculation are in progress in our laboratories to explain these unusual findings and propose mechanisms.

Exploiting (a) the Hard and Soft Acids and Bases (HSAB) model and (b) the tendency of Mebta (acting as ancillary ligand) to preferentially bind to divalent 3d-metal ions made possible the synthesis of heterometallic complexes. The “ingredients” were Hg(II) [a soft acid], the thiocyanato ligand (a soft base when coordinated through S and a “borderline” base when coordinated through N), Co(II) or Ni(II) [“borderline acids”] and occasionally chlorides or bromides. We have to date isolated and structurally characterized the 3D coordination polymer $\{[\text{HgCo}(\text{SCN})_4(\text{Mebta})_2]\}_n$ (**63**), and the 1D chain polymers $\{[\text{HgCo}(\text{SCN})_2\text{Cl}_2(\text{H}_2\text{O})_2(\text{Mebta})_2]\}_n$ (**64**), $\{[\text{HgCo}(\text{SCN})_2\text{Br}_2(\text{DMF})_2(\text{Mebta})_2]\}_n$ (**65**) and $\{[\text{HgNi}(\text{SCN})_2\text{Cl}_2(\text{MeOH})_2(\text{Mebta})_2]\}_n$ (**66**). For example, complex **66** was prepared by the reaction represented by Equation (28). Its molecular structure (Figure 49) consists of chains comprising alternating $\{\text{Ni}^{\text{II}}\text{Hg}^{\text{II}}\}$ units. Neighboring Hg^{II} and Ni^{II} atoms are bridged by one SCN^- ion, which coordinates to Ni^{II} through its N and to Hg^{II} through its S (as expected from HSAB considerations). Two monodentate Mebta ligands and two terminal MeOH molecules complete an octahedral environment for Ni^{II} , while two chloro groups are terminally bonded to Hg^{II} giving rise to tetrahedral coordination; thus, the coordination spheres are $\{\text{Ni}^{\text{II}}\text{N}_2\text{N}'_2\text{O}_2\}$ and $\{\text{Hg}^{\text{II}}\text{S}_2\text{Cl}_2\}$. The preference of chlorides to coordinate with Hg^{II} may be explained by the great covalency of the $\text{Hg}^{\text{II}}\text{-Cl}$ bond and the fact that such bonds already existed in the starting mercury(II) material (HgCl_2).



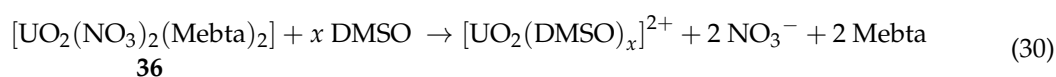
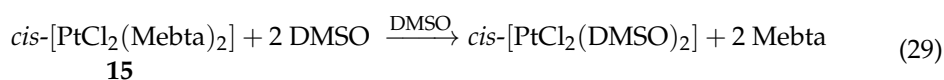
7. Concluding Remarks in Brief and Prognosis for the Future

In this work, we have comprehensively reviewed the to-date published metal complexes of Mebta with emphasis on their synthetic chemistry and important structural features. We have also briefly commented on unpublished work from our group. We hope that we have convinced the readers that Mebta is an interesting ligand. Its chemistry is distinctly different from that of other typical monodentate aromatic N-donors, such as pyridines and quinolines. The recently discovered (and not expected) bidentate N(2), N(3)-bridging behavior in compounds **28** [80], possibly **29** [92] and **38** (unpublished work) presages new clusters and coordination polymers in which the metal ions will be bridged by Mebta ligands; such complexes may have interesting properties, e.g., magnetic ones. The to-date developed “periodic table” of Mebta is shown in Figure 50. There are many metal/metalloid positions empty, justifying the title of the review (“Towards Construction. ...1-methylbenzotriazole”). We can easily see that no s-, p- (except In^{III}) and 4f-metal complexes have been reported. Our preliminary experiments show that no lanthanide(III) $[\text{Ln}^{\text{III}}]$ complexes of Mebta can be isolated. This may be due to the well-known inherent thermodynamic instability of the $\text{Ln}^{\text{III}}\text{-N}$ bond, especially in media containing low concentrations of water, either from the solvent or the metal starting materials. We are working hard to fill in as many as possible empty positions in the table. If we are successful, a future review in “Inorganics” will have the title “Towards Completion of the ‘Periodic Table’ of 1-methylbenzotriazole”!

1																	2
1 H hydrogen 1.0079																	2 He helium 4.0026
3 Li lithium 6.941	4 Be beryllium 9.01218											13 B boron 10.811	14 C carbon 12.0107	15 N nitrogen 14.0067	16 O oxygen 15.9994	17 F fluorine 18.9984	18 Ne neon 20.1797
11 Na sodium 22.9898	12 Mg magnesium 24.3050											13 Al aluminum 26.9815	14 Si silicon 28.0855	15 P phosphorus 30.9738	16 S sulfur 32.065	17 Cl chlorine 35.453	18 Ar argon 39.948
19 K potassium 39.0983	20 Ca calcium 40.078	21 Sc scandium 44.9559	22 Ti titanium 47.867	23 V vanadium 50.9415	24 Cr chromium 51.9961	25 Mn manganese 54.9280	26 Fe iron 55.845	27 Co cobalt 58.9332	28 Ni nickel 58.6934	29 Cu copper 63.546	30 Zn zinc 65.409	31 Ga gallium 69.723	32 Ge germanium 72.64	33 As arsenic 74.9216	34 Se selenium 78.96	35 Br bromine 79.904	36 Kr krypton 83.798
37 Rb rubidium 85.4678	38 Sr strontium 87.62	39 Y yttrium 88.9059	40 Zr zirconium 91.224	41 Nb niobium 92.9064	42 Mo molybdenum 95.96	43 Tc technetium (98)	44 Ru ruthenium 101.07	45 Rh rhodium 102.906	46 Pd palladium 106.42	47 Ag silver 107.868	48 Cd cadmium 112.411	49 In indium 114.818	50 Sn tin 118.710	51 Sb antimony 121.760	52 Te tellurium 127.60	53 I iodine 126.904	54 Xe xenon 131.293
55 Cs cesium 132.905	56 Ba barium 137.327	71 Lu lutetium 174.968	72 Hf hafnium 178.49	73 Ta tantalum 180.949	74 W tungsten 183.84	75 Re rhenium 186.207	76 Os osmium 190.23	77 Ir iridium 192.217	78 Pt platinum 195.084	79 Au gold 196.967	80 Hg mercury 200.59	81 Tl thallium 204.383	82 Pb lead 207.2	83 Bi bismuth 208.980	84 Po polonium (209)	85 At astatine (210)	86 Rn radon (222)
87 Fr francium (223)	88 Ra radium (226)	103 Lr lawrencium (262)	104 Rf rutherfordium (267)	105 Db dubnium (268)	106 Sg seaborgium (271)	107 Bh bohrium (272)	108 Hs hassium (270)	109 Mt meitnerium (276)	110 Ds darmstadtium (281)	111 Rg roentgenium (280)	112 Cn copernicium (285)	113 Nh nihonium (284)	114 Fl flerovium (289)	115 Mc moscovium (288)	116 Lv livermorium (293)	117 Ts tennessine (294)	118 Og oganesson (294)
57 La lanthanum 138.905	58 Ce cerium 140.116	59 Pr praseodymium 140.908	60 Nd neodymium 144.242	61 Pm promethium (145)	62 Sm samarium 150.36	63 Eu europium 151.964	64 Gd gadolinium 157.25	65 Tb terbium 158.925	66 Dy dysprosium 162.500	67 Ho holmium 164.930	68 Er erbium 167.259	69 Tm thulium 168.934	70 Yb ytterbium 173.04				
89 Ac actinium 227.027	90 Th thorium 232.038	91 Pa protactinium 231.036	92 U uranium 238.029	93 Np neptunium (237)	94 Pu plutonium (244)	95 Am americium (243)	96 Cm curium (247)	97 Bk berkelium (247)	98 Cf californium (251)	99 Es einsteinium (252)	100 Fm fermium (257)	101 Md mendelevium (258)	102 No nobelium (259)				

Figure 50. The present form of the “periodic table” of Mebta. Colour code: Red; metals whose complexes with Mebta have been published. Yellow; metals with unpublished coordination chemistry of Mebta.

Figure 50 refers to metal ions whose complexes with Mebta have been characterized in the solid state. We have also made an effort to understand if the solid-state structures of the complexes are retained in solution. The technique used for the complexes with diamagnetic metal ions was NMR spectroscopy (^1H and ^{13}C NMR), combined with the determination of molar conductivity values [3,86,95]. For solubility reasons, the solvent of choice was d_6 -DMSO. The results have provided strong evidence that the complexes decompose completely in solution releasing the coordinated Mebta molecules; the coordination sphere of the metal ions is filled with molecules of the solvent, which has a strong donor capacity. The decomposition schemes for the Zn(II) complexes [3] 30–33 were illustrated in part 5.9, Equation (25). The decomposition schemes for the complexes 15 [86] and 36 [95] are represented by Equations (29) and (30), respectively ($x = 5$ or 6):



Finally, we wish to make a short comment on the closely related (to Mebta), but less bulky compound 1-methyl-1,2,3-triazole (Meta, Figure 8). Meta also has different electronic properties than Mebta due to the absence of the benzene ring. To our great surprise, the coordination chemistry of Meta has been studied much less [92,96,97] being confined to Ag(I) [96,97] and Cu(I) [92]. There has been no published work on the s-, p- and f-block metal complexes with this ligand. The Ag(I) complex of Meta with the weakly coordinating anion PF_6^- , $[\text{Ag}(\text{Meta})_2](\text{PF}_6)$, is two-coordinate with a linear geometry [97], whereas

42 and **43** are three-coordinate (Figure 42). Notably, the addition of elemental iodine to $[\text{Ag}(\text{Meta})_2](\text{PF}_6)$ affords the corresponding linear iodonium complex $[\text{I}(\text{Meta})_2](\text{PF}_6)$ through the selective $[\text{N}-\text{Ag}^+-\text{N}] \rightarrow [\text{N}-\text{I}^+-\text{N}]$ cation exchange; we currently investigate if the reactions of **42** and **43** with I_2 can provide analogous iodonium species. On the contrary, $\{[\text{Cu}_2\text{I}_2(\text{Meta})]\}_n$ [92] seems to possess a similar molecular structure with its Mebta counterpart $\{[\text{Cu}_2\text{I}_2(\text{Mebta})]\}_n$ (**29**) [92]. We do believe that researchers should direct their efforts to investigate the coordination chemistry of Meta and compare it with that of Mebta.

Author Contributions: Conceptualization, C.T.C. and S.P.P.; resources, C.S. and S.P.; methodology, Z.G.L.; visualization, C.S.; writing-original draft preparation, C.T.C.; supervision, project administration, writing-review and editing, S.P.P. All authors have read and agreed to the published version of the manuscript.

Funding: This research received no external funding.

Acknowledgments: S.P.P. would like to thank Spyros Yiannopoulos for the purchase of a quantity of Mebta.

Conflicts of Interest: The authors declare no conflicts of interest.

References

1. Loukopoulos, E.; Kostakis, G. Recent advances in the coordination chemistry of benzotriazole-based ligands. *Coord. Chem. Rev.* **2019**, *395*, 193–229. [\[CrossRef\]](#)
2. Moore, D.S.; Robinson, S.D. Catenated Nitrogen Ligands Part II. Transition Metal Derivatives of Triazoles, Tetrazoles, Pentazoles, and Hexazine. *Adv. Inorg. Chem.* **1998**, *32*, 171–239.
3. Stamou, C.; Barouni, E.; Plakatouras, J.C.; Sigalas, M.M.; Raptopoulou, C.P.; Psycharis, V.; Bakalbassis, E.G.; Perlepes, S.P. The “Periodic Table” of 1-methylbenzotriazole: Zinc(II) Complexes. *Inorganics* **2023**, *11*, 356. [\[CrossRef\]](#)
4. Coxall, R.A.; Harris, S.G.; Henderson, D.K.; Parsons, S.; Tasker, P.A.; Winpenny, R.E.P. Inter-Ligand Reactions: In Situ Formation of New Polydentate Ligands. *J. Chem. Soc. Dalton Trans.* **2000**, *14*, 2349–2356. [\[CrossRef\]](#)
5. Aromi, G.; Barrios, L.A.; Roubeau, O.; Gamez, P. Triazoles and tetrazoles. Prime ligands to generate remarkable coordination materials. *Coord. Chem. Rev.* **2011**, *255*, 485–546. [\[CrossRef\]](#)
6. Constable, E.C. What’s in a Name?—A Short History of Coordination Chemistry from Then to Now. *Chemistry* **2019**, *1*, 126–133. [\[CrossRef\]](#)
7. Klement, R. Phosphorsäure als Ligand in Komplexen Kobaltverbindungen. *Z. Anorg. Allg. Chem.* **1926**, *156*, 237–244. [\[CrossRef\]](#)
8. Tsuchida, R. Absorption spectra of coordination compounds. I. *Bull. Chem. Soc. Jpn.* **1938**, *13*, 388–400. [\[CrossRef\]](#)
9. Tumaki, T. Coordinate valency rings. V. Spectrochemical researches on the inner complex metallic salts of salicylaldehyde-ethylenediimine and related compounds. *Bull. Chem. Soc. Jpn.* **1938**, *13*, 583–591.
10. IUPAC. *Nomenclature of Inorganic Chemistry, 1957 Report of CNIC*; Butterworths Scientific Publications: London, UK, 1959.
11. Constable, E.C. *Metals and Ligand Reactivity*; VCH: Weinheim, Germany, 1996; pp. 22–45.
12. Tomàs, F.; Abboud, J.-L.M.; Laynez, J.; Notario, R.; Santos, L.; Nilsson, S.O.; Catalàn, J.; Claramunt, R.M.; Elguero, J. Tautomerism and Aromaticity in 1,2,3-Triazoles: The Case of Benzotriazole. *J. Am. Chem. Soc.* **1989**, *111*, 7348–7353. [\[CrossRef\]](#)
13. Hall, C.D.; Panda, S.S. The Benzotriazole Story. *Adv. Heterocycl. Chem.* **2016**, *119*, 1–23.
14. Katritzky, A.R.; Belyakov, S.A. Benzotriazole-Based Intermediates: Reagents for Efficient Organic Synthesis. *Aldrichim. Acta* **1998**, *31*, 35–45.
15. Katritzky, A.R.; Rachwal, S.; Hitchings, G.J. Benzotriazole: A Novel Synthetic Auxiliary. *Tetrahedron* **1991**, *47*, 2683–2732. [\[CrossRef\]](#)
16. Katritzky, A.R. N-Substituted Benzotriazoles: Properties, Reactivities and Synthetic Utility. *Bull. Soc. Chim. Belg.* **1992**, *101*, 409–413. [\[CrossRef\]](#)
17. Briguglio, I.; Piras, S.; Corona, P.; Gavini, E.; Nieddu, M.; Boatto, G.; Carta, A. Benzotriazole: An overview on its versatile biological behavior. *Eur. J. Med. Chem.* **2015**, *97*, 612–648. [\[CrossRef\]](#)
18. Patel, P.K.; Patel, P.D.; Patel, S. Synthesis, Characterization, Chelating Properties and Biological Activities of Benzotriazole-Salicylic Acid Combined Molecule. *Int. J. Pharm. Chem. Sci.* **2012**, *1*, 1799–1804.
19. Oberley, L.W.; Buettner, G.R. Role of superoxide dismutase in cancer: A review. *Cancer Res.* **1979**, *39*, 1141–1149.
20. Kraševac, I.; Prosen, H. Solid-Phase Extraction of Polar Benzotriazoles as Environmental Pollutants: A Review. *Molecules* **2018**, *23*, 2501. [\[CrossRef\]](#)
21. Ding, J.; Yan, Z.; Feng, L.; Zhai, F.; Chen, X.; Xu, Y.; Tang, S.; Huang, C.; Li, L.; Pan, N.; et al. Benzotriazole decorated graphene oxide for efficient removal of U(VI). *Environ. Pollut.* **2019**, *253*, 221–230. [\[CrossRef\]](#)
22. Flippen-Anderson, J.L.; Gilardi, R.D.; Pitt, A.M.; Wilson, W.S. Synthesis and Explosive Properties of Benzotriazoles. *Aust. J. Chem.* **1992**, *45*, 513–524. [\[CrossRef\]](#)

23. Malow, M.; Wehrstedt, K.D.; Neuenfeld, S. On the explosive properties of 1H-benzotriazole and 1H, 1,2,3-triazole. *Tetrahedron Lett.* **2007**, *48*, 1233–1235. [\[CrossRef\]](#)
24. Srinivas, D.; Ghule, V.D.; Tewari, S.P.; Muralidharan, K. Synthesis of Amino, Azido, Nitro, and Nitrogen-Rich Azole-Substituted Derivatives of 1H-Benzotriazole for High-Energy Materials Applications. *Chem. Eur. J.* **2012**, *18*, 15031–15037. [\[CrossRef\]](#)
25. Paterson, M.J.; Robb, M.A.; Blancafort, L.; DeBellis, A.D. Theoretical Study of Benzotriazole UV Photostability: Ultrafast Deactivation through Coupled Proton and Electron Transfer Triggered by a Charge-Transfer State. *J. Am. Chem. Soc.* **2004**, *126*, 2912–2922. [\[CrossRef\]](#)
26. Lai, H.-J.; Ying, G.-G.; Ma, Y.-B.; Chen, Z.-F.; Chen, F.; Liu, Y.-S. Field dissipation and plant uptake of benzotriazole ultraviolet stabilizers in biosolid-amended soils. *Environ. Sci. Process. Impacts* **2014**, *16*, 558–566. [\[CrossRef\]](#)
27. Kiejza, D.; Karpińska, J.; Kotowska, U. Degradation of Benzotriazole UV Stabilizers in PAA/d-Electron Metal Ion Systems-Removal Kinetics, Products and Mechanism Evaluation. *Molecules* **2022**, *27*, 3349. [\[CrossRef\]](#)
28. Kokalj, A.; Peljhan, S.; Finšgar, M.; Milošev, I. What Determines the Inhibition Effectiveness of ATH, BTAH, and BTAOH Corrosion Inhibitors on Copper? *J. Am. Chem. Soc.* **2010**, *132*, 16657–16668. [\[CrossRef\]](#)
29. Grillo, F.; Tee, D.W.; Francis, S.M.; Früchti, H.; Richardson, N.V. Initial stages of benzotriazole adsorption on the Cu(111) surface. *Nanoscale* **2013**, *5*, 5269–5273. [\[CrossRef\]](#)
30. Kokalj, A. Ab initio modeling of the bonding of benzotriazole corrosion inhibitor to reduced and oxidized copper surfaces. *Faraday Discuss.* **2015**, *180*, 415–438. [\[CrossRef\]](#)
31. Gattinoni, C.; Michaelides, A. Understanding corrosion inhibition with van der Waals DFT methods: The case of benzotriazole. *Faraday Discuss.* **2015**, *180*, 439–458. [\[CrossRef\]](#) [\[PubMed\]](#)
32. Törnkvist, C.; Thierry, D.; Bergman, J.; Liedberg, B.; Leygraf, C. Methyl Substitution in Benzotriazole and Its Influence on Surface Structure and Corrosion Inhibition. *J. Electrochem. Soc.* **1989**, *136*, 58–64. [\[CrossRef\]](#)
33. Procter and Gamble Co. Compositions for Inhibiting Metal Tarnish. British Patent 652339, 8 November 1948.
34. Madsen, H.B. A Preliminary Note on the Use of Benzotriazole for Stabilizing Bronze Objects. *Stud. Conserv.* **1967**, *12*, 163–166. [\[CrossRef\]](#)
35. Sease, C. Benzotriazole: A Review for Conservators. *Stud. Conserv.* **1978**, *23*, 76–85. [\[CrossRef\]](#)
36. Walker, R. Benzotriazole, a Corrosion Inhibitor for Antiques. *J. Chem. Educ.* **1980**, *57*, 789–791. [\[CrossRef\]](#)
37. Catalán, J.; Claramunt, R.M.; Elguero, J.; Laynèz, J.; Menéndez, M.; Anvia, F.; Quian, J.H.; Taagepera, M.; Taft, R.W. Basicity and Acidity of Azoles: The Annulation Effect in Azoles. *J. Am. Chem. Soc.* **1988**, *110*, 4105–4111. [\[CrossRef\]](#)
38. Begtrup, M.; Elguero, J.; Faure, R.; Camps, P.; Estopá, C.; Ilavský, D.; Fruchier, A.; Marzin, C.; Mendoza, J.d. Effects of N-substituents on the ^{13}C NMR Parameters of Azoles. *Magn. Reson. Chem.* **1988**, *26*, 134–151. [\[CrossRef\]](#)
39. Claramunt, R.M.; Sanz, D.; Boyer, G.; Catalán, J.; Paz, J.L.G.d. Experimental (^{13}C and ^{15}N Spectroscopy) and Theoretical (6-31G) Study of the Protonation of N-Methylazoles and N-Methylbenzazoles. *Magn. Reson. Chem.* **1993**, *31*, 791–800. [\[CrossRef\]](#)
40. Novak, I.; Abu-Izneid, T.; Kovač, B.; Klasinc, L. Electronic Structure and Stability of Benzotriazoles. *J. Phys. Chem. A* **2009**, *113*, 9751–9756. [\[CrossRef\]](#)
41. Catalán, J.; Pérez, P.; Elguero, J. Structure of Benzotriazole in the Gas Phase: A UV Experimental Study. *J. Org. Chem.* **1993**, *58*, 5276–5277. [\[CrossRef\]](#)
42. Rondeau, R.E.; Rosenberg, H.M.; Dunbar, D.J. Nuclear Magnetic Resonance Analysis of 1- and 2-Methylbenzotriazole. *J. Mol. Spectr.* **1969**, *29*, 305–311. [\[CrossRef\]](#)
43. Thomas, S.; Venkateswaran, S.; Kapoor, S.; D’Cunha, R.; Mukherjee, T. Surface enhanced Raman scattering of benzotriazole: A molecular orientational study. *Spectrochim. Acta Part A* **2004**, *60*, 25–29. [\[CrossRef\]](#)
44. Aruchamy, A.; Fujishima, A.; Ibrahim, A.; Loo, B.H. A surface-enhanced Raman spectroscopic study of benzotriazole and 6-tolyltriazole corrosion inhibitors on copper electrodes in alkaline solutions. *J. Electroanal. Chem.* **1990**, *281*, 299–304. [\[CrossRef\]](#)
45. Sockalingum, D.; Fleischmann, M.; Musiani, M.M. Near-infrared Fourier transform surface-enhanced Raman scattering of azole copper corrosion inhibitors in aqueous chloride media. *Spectrochim. Acta Part A* **1991**, *47*, 1475–1485. [\[CrossRef\]](#)
46. Tangoulis, V.; Raptopoulou, C.P.; Terzis, A.; Bakalbassis, E.G.; Diamantopoulou, E.; Perlepes, S.P. Polynuclear Nickel(II) Complexes: Preparation, Characterization, Magnetic Properties, and Quantum-Chemical Study of $[\text{Ni}_5(\text{OH})(\text{Rbta})_5(\text{acac})_4(\text{H}_2\text{O})_4]$ (RbtaH = Benzotriazole and 5,6-Dimethylbenzotriazole). *Inorg. Chem.* **1998**, *37*, 3142–3153. [\[CrossRef\]](#)
47. Biswas, S.; Tonigold, M.; Volkmer, D. Homo- and Heteronuclear Coordination Compounds with T_d Symmetry- the Solid State Structures of $[\text{MZn}_4(\text{L})_4(\text{L}')_6]$ ($\text{M} = \text{Co}^{\text{II}}$ or Zn^{II} ; L = chloride or acac; L' = 1,2,3-benzotriazolate). *Z. Anorg. Allg. Chem.* **2008**, *634*, 2532–2538. [\[CrossRef\]](#)
48. Biswas, S.; Tonigold, M.; Speldrich, M.; Kögerler, P.; Volkmer, D. Nonanuclear Coordination Compounds Featuring $\{\text{M}_9\text{L}_{12}\}^{6+}$ Cores ($\text{M} = \text{Ni}^{\text{II}}$, Co^{II} , or Zn^{II} ; L = 1,2,3-Benzotriazolate). *Eur. J. Inorg. Chem.* **2009**, *2009*, 3094–3101. [\[CrossRef\]](#)
49. Biswas, S.; Tonigold, M.; Kelm, H.; Krüger, H.-J.; Volkmer, D. Thermal spin-crossover in the $[\text{M}_3\text{Zn}_6\text{Cl}_6\text{L}_{12}]$ ($\text{M} = \text{Zn}$, Fe^{II} ; L = 5,6-dimethoxy-1,2,3-benzotriazolate) system: Structural, electrochemical, Mössbauer, and UV-Vis spectroscopic studies. *Dalton Trans.* **2010**, *39*, 9851–9859. [\[CrossRef\]](#) [\[PubMed\]](#)
50. Biswas, S.; Tonigold, M.; Speldrich, M.; Kögerler, P.; Weill, M.; Volkmer, D. Syntheses and Magnetostructural Investigations on Kuratowski-Type Homo- and Heteropentanuclear Coordination Compounds $[\text{MZn}_4\text{Cl}_4(\text{L})_6]$ ($\text{M}_{\text{II}} = \text{Zn}$, Fe , Co , Ni , or Cu ; L = 5,6-Dimethyl-1,2,3-benzotriazolate) Represented by the Nonplanar $\text{K}_{3,3}$ Graph. *Inorg. Chem.* **2010**, *49*, 7424–7434. [\[CrossRef\]](#) [\[PubMed\]](#)

51. Xue, X.; Li, G.-T.; Peng, Y.-H.; Wu, L.; Wu, B.-L. Two photoluminescent pentanuclear homo- and hetero-metal complexes based on benzotriazole bridge. *J. Coord. Chem.* **2011**, *64*, 1593–1962. [\[CrossRef\]](#)
52. Liu, Y.-Y.; Grzywa, M.; Tonigold, M.; Sastre, G.; Schüttrigkeit, T.; Leeson, N.S.; Volkmer, D. Photophysical properties of Kuratowski-type coordination compounds $[M^{II}Zn_4Cl_4(Me_2bta)_6]$ ($M^{II} = Zn$ or Ru) featuring long-lived excited electronic states. *Dalton Trans.* **2011**, *40*, 5926–5938. [\[CrossRef\]](#)
53. Werner, T.W.; Reschke, S.; Bunzen, H.; Krug von Nidda, H.-A.; Deisenhofer, J.; Loidl, A.; Volkmer, D. $[Co_5Tp_4^*(Me_2bta)_6]$: A Highly Symmetrical Pentanuclear Kuratowski Complex Featuring Tris(pyrazolyl)borate and Benzotriazolate Ligands. *Inorg. Chem.* **2016**, *55*, 1053–1060. [\[CrossRef\]](#)
54. Bunzen, H.; Grzywa, M.; Kalytta-Mewes, A.; Volkmer, D. One-pot synthesis of ultrastable pentanuclear alkylzinc complexes. *Dalton Trans.* **2017**, *46*, 2613–2625. [\[CrossRef\]](#) [\[PubMed\]](#)
55. Zhou, G.-J.; Chen, W.-P.; Yu, Y.; Qin, L.; Han, T.; Zheng, Y.-Z. Filling the Missing Links of M_{3n} Prototype 3d-4f and 4f Cyclic Coordination Cages: Syntheses, Structures and Magnetic Properties of the $Ni_{10}Ln_5$ and the Er_{3n} Wheels. *Inorg. Chem.* **2017**, *56*, 12821–12829. [\[CrossRef\]](#) [\[PubMed\]](#)
56. Papatriantafyllopoulou, C.; Diamantopoulou, E.; Terzis, A.; Tangoulis, V.; Lalioti, N.; Perlepes, S.P. High-nuclearity nickel(II) clusters: Ni_{13} complexes from the use of 1-hydroxybenzotriazole. *Polyhedron* **2009**, *28*, 1903–1911. [\[CrossRef\]](#)
57. Andrews, P.C.; Clegg, W.; Mulvey, R.E.; O’Neil, P.A.; Wilson, M.M. An Infinite Ladder Structure of Alternating, Fused K_2N_2 Rhomboids and KN_2 Triangles: Synthesis and Crystallographic Characterization of Benzotriazolatopotassium-HPMA (HPMA = hexamethylphosphoric triamide). *J. Chem. Soc. Chem. Commun.* **1993**, 1142–1144. [\[CrossRef\]](#)
58. Müller-Buschbaum, K.; Mokaddem, Y. Rare Earth Benzotriazoles: Coordination Polymers Incorporating Decomposition Products from Ammonia to 1,2-Diaminobenzene in $1/\infty [Ln(Btz)_3(BtzH)]$ ($Ln = Ce, Pr$), $1/\infty [Ln(Btz)_3(Ph(NH_2)_2)]$ ($Ln = Nd, Tb, Yb$), and $1/\infty [Ho_2(Btz)_6(BtzH)(NH_3)]$. *Eur. J. Inorg. Chem.* **2006**, *2006*, 2000–2010. [\[CrossRef\]](#)
59. Müller-Buschbaum, K.; Mokaddem, Y. MOFs by Transformation of 1D-Coordination Polymers: From $1/\infty [Ln(Btz)_3BtzH]$ to the Homoleptic Rare Earth 3D-Benzotriazolate Frameworks $3/\infty [Ln(Btz)_3]$, $Ln = La, Ce$. *Z. Anorg. Allg. Chem.* **2008**, *634*, 2360–2366. [\[CrossRef\]](#)
60. Biswas, S.; Grzywa, M.; Nayek, H.P.; Dehnen, S.; Senkovska, I.; Kaskel, S.; Volkmer, D. A cubic coordination framework constructed from benzobistriazolate ligands and zinc ions having selective gas sorption properties. *Dalton Trans.* **2009**, *33*, 6487–6495. [\[CrossRef\]](#) [\[PubMed\]](#)
61. Xia, J.; Liu, B.-Y.; Wei, G.; Huang, X.-C. Solvent Induced Diverse Dimensional Coordination Assemblies of Cupric Benzotriazole-5-carboxylate: Syntheses, Crystal Structures, and Magnetic Properties. *Inorg. Chem.* **2011**, *50*, 11032–11038. [\[CrossRef\]](#) [\[PubMed\]](#)
62. Li, Z.-H.; Xue, L.-P.; Zhao, B.-T.; Kan, J.; Su, W.-P. 2D lanthanide-organic frameworks constructed from lanthanide acetate skeletons and benzotriazole-5-carboxylic acid connectors: Synthesis, structure, luminescence and magnetic properties. *Cryst. Eng. Commun.* **2012**, *14*, 8485–8491. [\[CrossRef\]](#)
63. Li, Z.-H.; Hong, D.-F.; Xue, L.-P.; Fu, W.-J.; Zhao, B.-T. Two lanthanide-bound 1H-benzotriazole polymers: New potential metal-organic scaffold for solid-phase organic chemistry. *Inorg. Chim. Acta* **2013**, *400*, 239–243. [\[CrossRef\]](#)
64. Schmieder, P.; Denysenko, D.; Grzywa, M.; Baumgärtner, B.; Senkovska, I.; Kaskel, S.; van Wüllen, L.; Volkmer, D. CFA-1: The first chiral metal-organic framework containing Kuratowski-type secondary building units. *Dalton Trans.* **2013**, *42*, 10786–10797. [\[CrossRef\]](#) [\[PubMed\]](#)
65. Sun, C.-Y.; Zhou, D.; Li, Y.; Li, W.-J.; Kang, Z.-T. Syntheses, Structures, and Fluorescent Properties of Lanthanide Complexes Based on the Ligand Benzotriazole-5-carboxylic Acid. *Z. Anorg. Allg. Chem.* **2014**, *640*, 2498–2502. [\[CrossRef\]](#)
66. Liu, J.; Zhang, H.-B.; Tan, Y.-X.; Wang, F.; Zhang, Y.; Zhang, J. Structural Diversity and Photoluminescent Properties of Zinc Benzotriazolate-5-carboxylate Coordination Polymers. *Inorg. Chem.* **2014**, *53*, 1500–1506. [\[CrossRef\]](#) [\[PubMed\]](#)
67. Bunzen, H.; Grzywa, M.; Hambach, M.; Spirk, S.; Volkmer, D. From Micro to Nano: A Toolbox for Tuning Crystal Size and Morphology of Benzotriazolate-Based Metal-Organic Frameworks. *Cryst. Growth Des.* **2016**, *16*, 3190–3197. [\[CrossRef\]](#)
68. Brede, F.A.; Mühlbach, F.; Sextl, G.; Müller-Buschbaum, K. Mechanochemical and thermal formation of 1H-benzotriazole coordination polymers and complexes of 3d-transition metals with intriguing dielectric properties. *Dalton Trans.* **2016**, *45*, 10609–10619. [\[CrossRef\]](#)
69. Xie, W.; Qin, J.-S.; He, W.-W.; Shao, K.-Z.; Su, Z.-M.; Du, D.-Y.; Li, S.-L.; Lan, Y.-Q. Encapsulation of an iridium complex in a metal-organic framework to give a composite with efficient white light emission. *Inorg. Chem. Front.* **2017**, *4*, 547–552. [\[CrossRef\]](#)
70. Xie, W.; Ning, S.; Zhang, Y.; Tang, Z.; Zhang, S.; Tang, R. A 3D supramolecular network as highly selective and sensitive luminescent sensor for PO_4^{3-} and Cu^{2+} ions in aqueous media. *Dyes Pigm.* **2018**, *150*, 36–43. [\[CrossRef\]](#)
71. Feng, X.; Guo, N.; Li, R.; Chen, H.; Ma, L.; Li, Z.; Wang, L. A facile route for tuning emission and magnetic properties by controlling lanthanide ions in coordination polymers incorporating mixed aromatic carboxylate ligands. *J. Solid State Chem.* **2018**, *268*, 22–29. [\[CrossRef\]](#)
72. Bunzen, H.; Grzywa, M.; Aljohani, R.; von Nidda, H.-A.K.; Volkmer, D. Synthesis, Thermal Stability and Magnetic Properties of a Manganese(II) Coordination Framework Containing Bistriazolate Ligands. *Eur. J. Inorg. Chem.* **2019**, *2019*, 4471–4476. [\[CrossRef\]](#)
73. Zhang, Q.-Y.; An, X.; Xu, L.; Yan, J.-H.; Zhang, S.; Xie, W.; Su, Z.-M. Syntheses, structure and properties of an especially stable Cd metal-organic framework driven by benzotriazole-5-carboxylic acid. *Inorg. Chem. Commun.* **2020**, *112*, 107726. [\[CrossRef\]](#)

74. Tangoulis, V.; Raptopoulou, C.P.; Psycharis, V.; Terzis, A.; Skorda, K.; Perlepes, S.P.; Cador, O.; Kahn, O.; Bakalbassis, E.G. Ferromagnetism in an Extended Three-Dimensional, Diamond-like Copper(II) Network: A New Copper(II)/1-hydroxybenzotriazole Complex Exhibiting Soft-Magnet Properties and two Transitions at 6.4 and 4.4 K. *Inorg. Chem.* **2000**, *39*, 2522–2529. [\[CrossRef\]](#)
75. Palmer, M.H.; Findlay, R.H.; Kennedy, S.M.F.; McIntyre, P.S. Reactivity of Indazoles and Benzotriazole towards N-Methylation and Analysis of the ^1H Nuclear Magnetic Resonance Spectra of Indazoles and Benzotriazoles. *J. Chem. Soc. Perkin II* **1975**, *7*, 1695–1700. [\[CrossRef\]](#)
76. Katritzky, A.R.; Kuzmierkiewicz, W.; Greenhill, J.V. An improved method for the N-alkylation of benzotriazole and 1,2,4-triazole. *Recl. Trav. Chim. Pays-Bas* **1991**, *110*, 369–373. [\[CrossRef\]](#)
77. Dimitropoulos, A.; Stamou, C.; Perlepes, S.P.; Lada, Z.G.; Petsalakis, I.D.; Marinakis, S. A study of 1-Methylbenzotriazole (MEBTA) Using Quantum Mechanical Calculations and Vibrational, Electronic and Nuclear Magnetic Resonance Spectroscopies. *J. Eng. Sci. Technol. Rev.* **2023**, *16*, 77–84. [\[CrossRef\]](#)
78. Mudzakir, A.; Liebing, P.; Haak, E.; Fischer, A.; Hilfert, L.; Goldhahn, R.; Edelman, F.T. An unusual phosphide addition reaction of 1,3-dimethyl-1,2,3-benzotriazolium iodide. *Inorg. Chem. Commun.* **2024**, *161*, 111924. [\[CrossRef\]](#)
79. Fang, B.-S.; Olson, C.G.; Lynch, D.W. A Photoemission Study of Benzotriazole on Clean Copper and Cuprous Oxide. *Surf. Sci.* **1986**, *176*, 476–490. [\[CrossRef\]](#)
80. Bortoluzzi, M.; Castro, J.; Girotto, M.; Enrichi, F.; Vomiero, A. Luminescent copper(I) coordination polymer with 1-methyl-1H-benzotriazole, iodide and acetonitrile as ligands. *Inorg. Chem. Commun.* **2019**, *102*, 141–146. [\[CrossRef\]](#)
81. Jones, L.F.; O'Dea, L.; Offermann, D.A.; Jensen, P.; Moubaraki, B.; Murray, K.S. Benzotriazole based 1-D, 2-D and 3-D metal dicyanamide and tricyanomethanide coordination networks. *Polyhedron* **2006**, *25*, 360–372. [\[CrossRef\]](#)
82. Plakatouras, J.C.; Bakas, T.; Huffman, C.J.; Huffman, J.C.; Papaefthymiou, V.; Perlepes, S.P. Two Different Terminal Nitrate Bonding Modes in $[\text{Fe}_2\text{O}(\text{NO}_3)_4(\text{C}_7\text{H}_7\text{N}_3)_4]$. *J. Chem. Dalton Trans.* **1994**, 2737–2738. [\[CrossRef\]](#)
83. Anastasiadis, N.C.; Bilis, G.; Plakatouras, J.C.; Raptopoulou, C.P.; Psycharis, V.; Beavers, C.; Teat, S.J.; Louloudi, M.; Perlepes, S.P. Iron(III) chloride-benzotriazole adducts with trigonal bipyramidal geometry: Spectroscopic, structural and catalytic studies. *Polyhedron* **2013**, *64*, 189–202. [\[CrossRef\]](#)
84. Plakatouras, J.C.; Perlepes, S.P.; Mentzafos, D.; Terzis, A.; Bakas, T.; Papaefthymiou, V. Coordination Chemistry of Corrosion Inhibitors of the Benzotriazole Type: Preparation and Characterization of Cobalt(II) Complexes with 1-methylbenzotriazole (Mebta) and the Crystal Structures of $[\text{CoCl}_2(\text{Mebta})_2]$, $\text{trans}[\text{Co}(\text{NCS})_2(\text{Mebta})_4]$, $\text{trans}[\text{Co}(\text{NCS})_2(\text{MeOH})_2(\text{Mebta})_2]$ and $\text{cis}[\text{Co}(\text{NO}_3)_2(\text{Mebta})_2]$. *Polyhedron* **1992**, *11*, 2657–2672.
85. Diamantopoulou, E.; Zafiroopoulos, T.F.; Perlepes, S.P.; Raptopoulou, C.P.; Terzis, A. Synthetic and Structural Chemistry of Nickel(II)/1-methylbenzotriazole Complexes. *Polyhedron* **1994**, *13*, 1593–1608. [\[CrossRef\]](#)
86. Kovala-Demertzi, D.; Perlepes, S.P. Coordination compounds of palladium(II) and platinum(II) with benzotriazoles. *Transition Met. Chem.* **1994**, *19*, 7–11. [\[CrossRef\]](#)
87. Skorda, K.; Perlepes, S.P.; Raptopoulou, C.P.; Keuleers, R.; Terzis, A.; Plakatouras, J. A structural model for the copper(II) site of Cu-Zn superoxide dismutase: Preparation, crystal structure and properties of $[\text{Cu}(\text{Mebta})_4(\text{H}_2\text{O})](\text{ClO}_4)_2 \cdot 0.4\text{EtOH}$ (Mebta = 1-methylbenzotriazole). *Transition Met. Chem.* **1999**, *24*, 541–545. [\[CrossRef\]](#)
88. Skorda, K.; Bakalbassis, E.G.; Mrozinski, J.; Perlepes, S.P.; Raptopoulou, C.P.; Terzis, A. Copper(II) Chloride-1-Methylbenzotriazole Chemistry: Variation of Product as a Function of Metal-to-Ligand Reaction Ratio; Synthesis, Structure and Properties of a Dinuclear Complex and a Novel Chain Polymer with two Alternating Chromophores. *J. Chem. Soc. Dalton Trans.* **1995**, 2317–2319. [\[CrossRef\]](#)
89. Skorda, K.; Stamatatos, T.C.; Vafiadis, A.P.; Lithoxidou, A.T.; Terzis, A.; Perlepes, S.P.; Mrozinski, J.; Raptopoulou, C.P.; Plakatouras, J.C.; Bakalbassis, E.G. Copper(II) chloride/1-methylbenzotriazole chemistry: Influence of various synthetic parameters on the product identity, structural and magnetic characterization, and quantum-chemical studies. *Inorg. Chim. Acta* **2005**, *358*, 562–582. [\[CrossRef\]](#)
90. Skorda, K.; Keuleers, R.; Terzis, A.; Raptopoulou, C.P.; Perlepes, S.P.; Plakatouras, J.C. Copper(II) bromide/1-methylbenzotriazole chemistry. Variation of product as a function of solvent and ligand-to-metal reaction ratio. *Polyhedron* **1999**, *18*, 3067–3075. [\[CrossRef\]](#)
91. Lazari, G.; Grammatikopoulos, S.; Perlepes, S.P.; Stamatatos, T.C. Combining benzotriazoles and azides in copper(II) chemistry: Synthesis, structural and spectroscopic characterization of a 1-D corrugated tape $[\text{Cu}(\text{N}_3)_2(1\text{-Mebta})]_n$ coordination polymer (1-Mebta = 1-methylbenzotriazole). *J. Coord. Chem.* **2021**, *74*, 1823–1833. [\[CrossRef\]](#)
92. Wu, T.; Li, M.; Li, D.; Huang, X.-C. Anions Cu_nI_n Cluster-Based Architectures Induced by In Situ Generated N-Alkylated Cationic Triazolium Salts. *Cryst. Growth Des.* **2008**, *8*, 568–574. [\[CrossRef\]](#)
93. Geary, W.J. The use of conductivity measurements in organic solvents for the characterization of coordination compounds. *Coord. Chem. Rev.* **1971**, *7*, 81–122. [\[CrossRef\]](#)
94. Li, X.; Xie, X.; Sun, N.; Liu, Y. Gold-Catalyzed Cadiot-Chodkiewicz-Type Cross-Coupling of Terminal Alkynes with Alkynyl Hypervalent Iodine Reagents: Highly Selective Synthesis of Unsymmetrical 1,3-Diynes. *Angew. Chem. Int. Ed.* **2017**, *56*, 6994–6998. [\[CrossRef\]](#)
95. Tsantis, S.T.; Mouzakitis, M.; Savvidou, A.; Raptopoulou, C.P.; Psycharis, V.; Perlepes, S.P. The “periodic table” of benzotriazoles: Uranium(VI) complexes. *Inorg. Chem. Commun.* **2015**, *59*, 57–60. [\[CrossRef\]](#)

-
96. Ward, J.S.; Frontera, A.; Rissanen, K. Utility of Three-Coordinate Silver Complexes Toward the Formation of Iodonium Ions. *Inorg. Chem.* **2021**, *60*, 5383–5390. [[CrossRef](#)]
 97. Yu, S.; Kumar, P.; Ward, J.S.; Frontera, A.; Rissanen, K. A “nucleophilic” iodine in a halogen-bonded iodonium complex manifests an unprecedented $I^+ \cdots Ag^+$ interaction. *Chem* **2021**, *7*, 948–958. [[CrossRef](#)]

Disclaimer/Publisher’s Note: The statements, opinions and data contained in all publications are solely those of the individual author(s) and contributor(s) and not of MDPI and/or the editor(s). MDPI and/or the editor(s) disclaim responsibility for any injury to people or property resulting from any ideas, methods, instructions or products referred to in the content.